A Case Study of Processes Impacting Precipitation Phase and Intensity during the Vancouver 2010 Winter Olympics

JULIE M. THÉRIAULT,*,+ ROY RASMUSSEN,+ TREVOR SMITH,# RUPING MO,#
JASON A. MILBRANDT,@ MELINDA M. BRUGMAN,# PAUL JOE,& GEORGE A. ISAAC,&
JOCELYN MAILHOT,@ AND BERTRAND DENIS**

+ *National Center for Atmospheric Research, Boulder, Colorado*
# *Meteorological Service of Canada, Environment Canada, Vancouver, British Columbia, Canada*
@ *Atmospheric Numerical Prediction Research, Environment Canada, Montreal, Quebec, Canada*
& *Cloud Physics and Severe Weather Research Section, Environment Canada, Toronto, Ontario, Canada*
** *National Predictions Development Division, Canadian Meteorological Center, Dorval, Quebec, Canada*

(Manuscript received 16 September 2011, in final form 10 May 2012)

ABSTRACT

Accurate forecasting of precipitation phase and intensity was critical information for many of the Olympic venue managers during the Vancouver 2010 Olympic and Paralympic Winter Games. Precipitation forecasting was complicated because of the complex terrain and warm coastal weather conditions in the Whistler area of British Columbia, Canada. The goal of this study is to analyze the processes impacting precipitation phase and intensity during a winter weather storm associated with rain and snow over complex terrain. The storm occurred during the second day of the Olympics when the downhill ski event was scheduled. At 0000 UTC 14 February, 2 h after the onset of precipitation, a rapid cooling was observed at the surface instrumentation sites. Precipitation was reported for 8 h, which coincided with the creation of a nearly 0°C isothermal layer, as well as a shift of the valley flow from up valley to down valley. Widespread snow was reported on Whistler Mountain with periods of rain at the mountain base despite the expectation derived from synoptic-scale models (15-km grid spacing) that the strong warm advection would maintain temperatures above freezing. Various model predictions are compared with observations, and the processes influencing the temperature, wind, and precipitation types are discussed. Overall, this case study provided a well-observed scenario of winter storms associated with rain and snow over complex terrain.

1. Introduction

A major challenge in winter weather forecasting is determining the occurrence and phase of precipitation over complex terrain. Predicting the precise type of precipitation and its intensity is an everyday challenge during winter in mountainous regions. Weather conditions may affect the available water resources in the spring, cause flooding, interrupt transportation, and affect outdoor activities. Accurate forecasts were especially challenging to perform during the Vancouver 2010 Winter Olympics in British Columbia, Canada, because the forecast requirements were tied to some specific critical weather thresholds for fair and safe competitions (Joe et al. 2010; Mailhot et al. 2010; Isaac et al. 2012, hereafter IPAG; Mo et al. 2012). The factors governing whether rain or snow will occur at the surface depend on the terrain when the 0°C isotherm is near the surface. In general, snowflakes in the atmosphere begin to melt as they fall into a melting layer where temperature varies between 0° and 4°C. Over flat terrain, Wexler et al. (1954) showed that rain can change to snow due to the diabatic cooling effects of melting in the atmosphere. It has long been known that the melting of snow often leads to an isothermal layer at 0°C (Findeisen 1940). Over sloped terrain, this thermodynamic effect combined with orographic

* Current affiliation: Département des Sciences de la Terre et de l'Atmosphère, Université du Québec à Montréal, Montreal, Quebec, Canada.

Corresponding author address: Julie M. Thériault, Case Postale 8888, Succursale Centreville, Montreal QC H3C 3P8, Canada.
E-mail: theriault.julie@uqam.ca

DOI: 10.1175/WAF-D-11-00114.1

factors can cause the 0°C isotherm to bend down toward the mountain surface (Marwitz 1987). Lumb (1983a,b) showed that this process is also enhanced by the adiabatic cooling associated with the vertical ascent of air moving up the barrier.

The characterization of the rain–snow boundary in mountainous terrain has been recently addressed in many studies. Based on data collected from the Mesoscale Alpine Program (MAP; Steiner et al. 2003) and the Improvement of Microphysical Parameterization through Observational Verification Experiment (IMPROVE; Stoelinga et al. 2003), Medina et al. (2005) identified similar patterns in the cross-barrier flow and precipitation associated with a radar bright band in both the European Alps and the Cascade Mountains in the United States. For hydrological applications, Lundquist et al. (2008) linked surface observations with the melting snow level aloft over complex terrain. Their results provide critical information for accurate runoff forecasting during precipitation events. Minder et al. (2011) have recently performed numerical simulation to study the mesoscale features of the rain–snow boundary along mountainside. They demonstrated that diabatic cooling of melting precipitation and adiabatic cooling from vertical motion influence the location of the rain–snow boundary along the mountainside. Their study also shows high uncertainty in the results based on different microphysical parameterizations. This is a critical issue because the determination of the precise phase of precipitation is sensitive to the temperature and vice versa. The change in temperature can affect the flow field in the vicinity of the rain–snow boundary, which, in turn, can alter the temperature. These feedback mechanisms are supported by observations collected in the Alps during the MAP field campaign. For example, Steiner et al. (2003) demonstrated that a down-valley flow occurred with a change in precipitation phase from snow to rain. However, Zängl (2007) suggested that melting contributed only modestly to this down-valley flow.

During the first week of the Vancouver 2010 Winter Olympics, a storm occurred that was associated with a rain–snow transition region along the mountainside. On 13 February 2010, the men's downhill ski race was postponed until 15 February because of the warm and rainy conditions in the Whistler area. One of the forecasting challenges was determining the relative importance of large-scale warm-air advection associated with a frontal passage through the region as compared to diabatic cooling of melting snow. Unterstrasser and Zängl (2006) showed that the balance between warm-air advection and diabatic cooling by melting over complex terrain is subtle because a small change in the atmospheric conditions will influence the importance of diabatic cooling. Because the temperature was near 0°C, the precipitation type could be either rain or snow. The correct discrimination of precipitation type was critical for officials to conduct a fair and safe competition.

Given the difficulties in predicting storms associated with a rain–snow transition region, the different atmospheric processes governing the precipitation phase and intensity of a winter storm in complex terrain are examined in this paper. The analysis will focus on whether diabatic cooling of melting snow played an important role on the precipitation types and low-level wind shift in the Whistler area. Other processes such as adiabatic effects, large-scale temperature advection, and flow blocking are also discussed.

This case study was conducted using the data available from a research and development project called the Science of Nowcasting Olympic Weather for Vancouver 2010 (SNOW-V10; IPAG). Many weather stations were installed in the Vancouver–Whistler area (Fig. 1). The observations were compared in real time with the forecast from a high-resolution (1-km grid spacing) configuration of the Canadian Global Environmental Multiscale (GEM) model used during the Vancouver 2010 Winter Olympics (Mailhot et al. 2010, 2012, hereafter MPAG). In addition, 1D simulations were also conducted to demonstrate the impact of diabatic cooling of melting snow.

The paper is organized as follows. Section 2 presents the weather forecast challenge facing Olympic forecasters. A synoptic overview of the storm is described in section 3. An analysis of the weather conditions in the Whistler area is given in section 4. Section 5 compares model guidance with observations. The results are compared with one-dimensional model simulations in section 6. Concluding remarks are given in section 7.

2. The Olympic forecast challenge

a. General geography and meteorology

The Vancouver–Whistler area is located along the south coast of British Columbia, Canada. It is associated with the very complex terrain of the Coast Mountains and is located in close proximity to the ocean (see Fig. 1). In winter, frontal systems embedded in a predominantly westerly airflow from the Pacific Ocean interact with the coastal mountains to produce varying amounts of precipitation in the form of rain or snow depending on elevation and proximity to the ocean.

During in situ venue training exercises in the three winters preceding the Vancouver 2010 Winter Olympics, forecasters soon discovered the difficulty of forecasting precipitation phase. They observed that the elevation of the rain–snow transition zone was often located near the elevation of the Olympic alpine venues. Determining the relative strength of warm-air advection

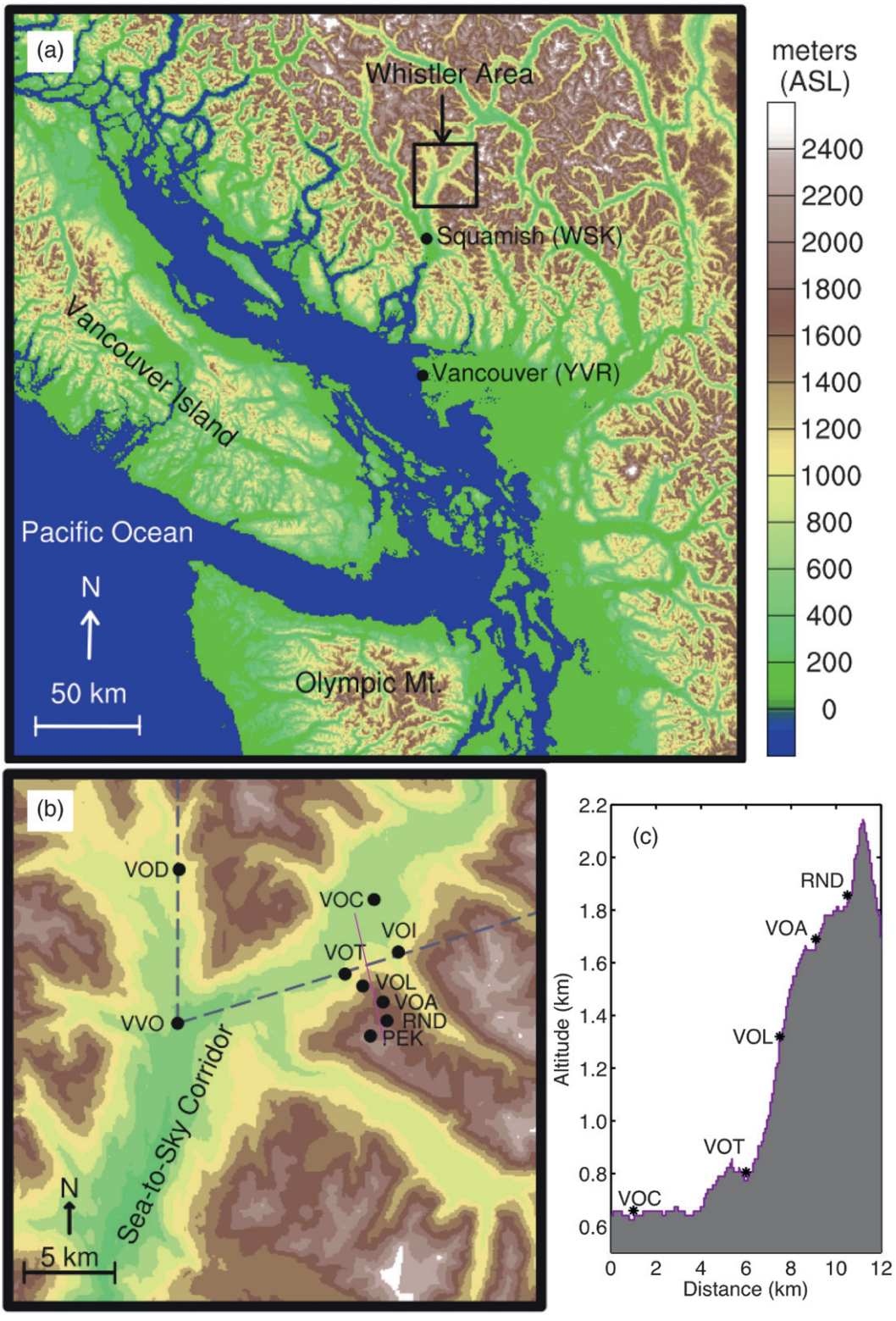

FIG. 1. (a) Geographical setting of the Vancouver 2010 Winter Olympics. (b) Orography of the Whistler area. (c) Cross section of Whistler Mountain. The locations of some weather stations are indicated. VVO is the location of the Whistler radar, VOD is in Callaghan Valley; the soundings were launched from VOC. In (b), the dashed lines show the 0° and 73° radar cross sections, and the pink solid line shows the cross section of topography in (c).

and diabatic processes was also identified as an important consideration to accurately forecast the elevation of the rain–snow transition zone.

b. *Science of nowcasting Olympic weather for Vancouver 2010*

Scientific advancements were needed to understand and accurately predict the weather during the Vancouver 2010 Winter Olympics. Therefore, many research sites were installed and equipped with advanced weather instruments. High-resolution models were configured as additional forecasting tools (Mailhot et al. 2010, MPAG). A detailed description of the field campaign is given in Joe et al. (2010, 2012, hereafter JPAG).

The forecasting and nowcasting of winter weather during the Vancouver 2010 Winter Olympic Games were supported by a group of operational forecasters and scientists. The operational forecasters deployed during the Games came from the Meteorological Service of Canada, the U.S. National Weather Service office, and the private Canadian Weather Network. The Olympic meteorologists training for the Games consisted of in situ venue forecasting exercises during the three winters preceding the 2010 Games. In addition to the practical forecasting experience, Olympic meteorologists received classroom lectures on theoretical mountain meteorology.

The orography of the Whistler area, including the numerous weather stations installed for the field campaign, is illustrated in Fig. 1b. Each of these weather stations has a three-letter identifier (e.g., VOC). This notation will be used throughout the paper. In particular, to meet the observational needs in the Whistler area, the operational weather instruments were supplemented by research instruments (appendix A). Further details are given in JPAG. These included high-frequency temperature, pressure, wind and precipitation intensity sensors. Due to the lack of AC power in the Callaghan Valley, no advanced precipitation sensors were installed at that location. Besides the conventional observations, some research sites were equipped with specialized instruments such as disdrometers, vertically pointing radars, and visibility and high-resolution precipitation intensity and type instruments. A C-band Doppler radar was located at VVO (Fig. 1b), which provided useful information about precipitation and Doppler wind fields over the area. In addition, soundings were launched daily from VOC (Fig. 1b) at 0000, 0600, 1200, and 1800 UTC, respectively.

To provide numerical weather prediction (NWP) model guidance to the forecasting team, Environment Canada (EC) ran a special high-resolution configuration of the Global Environmental Multiscale (GEM) model. Twice daily, a set of one-way nested forecast grids were integrated, starting from the Canadian Meteorological Centre (CMC) regional analysis, running a variable-resolution global forecast (with a 15-km horizontal grid spacing over Canada), then cascading to 15-, 2.5-, and 1-km limited-area model (LAM) grids centered over the Vancouver–Whistler region. The 15-km cascade of the LAM is needed to spin up for the 2.5-km grid in order to include hydrometeor fields. Details of the GEM model can be found in Côté et al. (1998) and a full description of the experimental model configuration for the Vancouver 2010 Winter Olympics is given in Mailhot et al. (2010). In all of the grids in the experimental system, cloud microphysical processes and precipitation were parameterized using the full double-moment version of the bulk microphysics scheme described in Milbrandt and Yau (2005a,b) (appendix B). Results from the 1-km integration (hereafter referred to as the GEM-LAM 1-km) are presented in section 5.

These high-resolution model forecasts were compared in real time with the observations recorded every minute at the weather stations. Both the model and the high-density observation sites provided valuable information on the current and forecast conditions needed during the Vancouver 2010 Winter Olympics. Each station was associated with the model grid point that would closely represent the meteorological conditions at that position. The model grid point was adjusted depending on the spatial resolution (appendix B).

3. Synoptic overview

The challenge of nowcasting the precipitation phase and intensity was crucial during the first weekend of the Vancouver 2010 Winter Olympics (13–14 February 2010). The downhill ski event and training were scheduled during that weekend but the warm and rainy weather forced the Olympic committee to postpone the event. The ski event was held between the weather stations named VOA (1640 m MSL) and VOT (805 m MSL) along Whistler Mountain (Creekside). A cross section of Whistler Mountain with the locations of the stations is given in Fig. 1c.

On 13 February 2010, an intense frontal system slowly approached the coastline of British Columbia as it elongated in a north–south orientation. The infrared [Geostationary Operational Environmental Satellite (*GOES-West*) 11 μm] image (Fig. 2) shows an elongated front wrapping into a deep 958-hPa low pressure region centered over the Gulf of Alaska. The frontal system was characterized by a narrow band of concentrated moisture in the lower troposphere, which could be considered to be an atmospheric river (Zhu and Newell 1998; Ralph et al. 2004). The northern extension of this frontal system was analyzed as a trough of warm air aloft (TROWAL). This feature directed warm moist air from

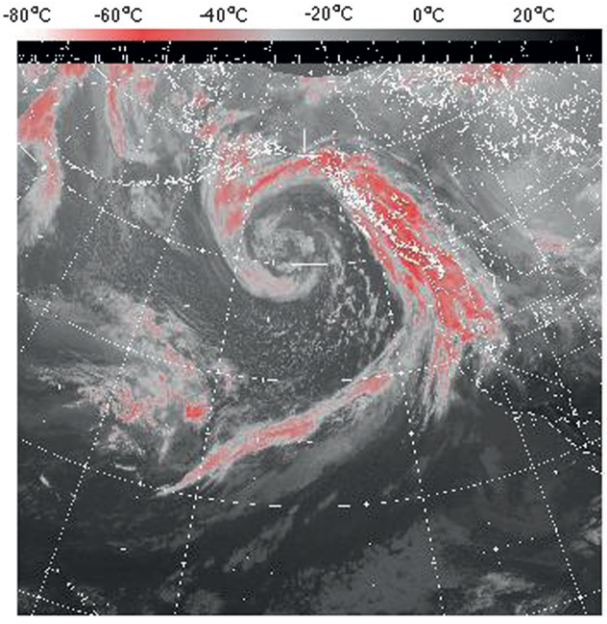

FIG. 2. Satellite infrared image (*GOES-11*) at 0000 UTC 14 Feb 2010.

the south along the west coast of North America. This large-scale forcing produced a strong low-level jet ahead of the frontal system, bringing south-to-southeasterly surface winds. The warm and moist air advected along the frontal system from the Pacific Ocean toward the mountainous terrain. The 0000 UTC 850-hPa map (Fig. 3) shows the warm air pushing northward along the TROWAL, which was located near the axis of maximum warmth aloft.

Given this intense atmospheric river system, relatively warm and wet weather was expected in the Whistler area where the downhill ski event was held. At 0000 UTC 14 February 2010, the forecasters had to predict the evolution of the phase and intensity of the precipitation for the day. The task was challenging due to temperatures near 0°C, winds, and the precipitation rate forecasted by the models. The model forecasts at the Roundhouse research station (RND) near the top of Whistler Mountain (Gultepe et al. 2012) are compared to observations in Fig. 4. The same comparison near the base of Whistler Mountain (VOT) is shown in Fig. 5. Note that the observations are shown up to 0000 UTC 14 February 2010 because the meteograms were available at the time. The GEM-LAM 15-km models were initialized at 1200 UTC 13 February 2010, the GEM-LAM 2.5-km model was initialized at 1500 UTC from the GEM-LAM 15-km model 3-h forecast, and then the GEM-LAM 1-km model was initialized at 2000 UTC from the GEM-LAM 2.5-km model 5-h forecast. Data used in Figs. 4 and 5 are 3-min outputs. The forecasters had the model guidance available at least up to 1200 UTC 14 February 2010, but the observations were only available until 0000 UTC 14 February 2010. A detailed comparison with the model outputs is discussed in section 4. The model grid points compared with the actual geographical location of each site are discussed in appendix B.

The model guidance suggested heavy precipitation in the Whistler area (Figs. 4a and 5a). The temperatures along the mountainside were forecasted around 0°C throughout the day (Figs. 4b and 5b). Near the top of

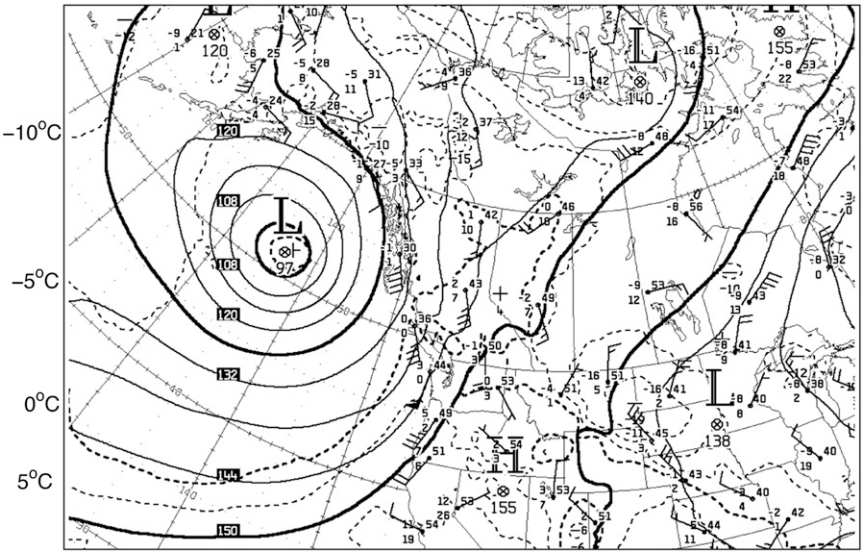

FIG. 3. The CMC Regional (REG) analysis of 850-hPa geopotential heights (dam, solid lines) and temperatures (°C, dashed lines) at 0000 UTC 14 Feb 2010.

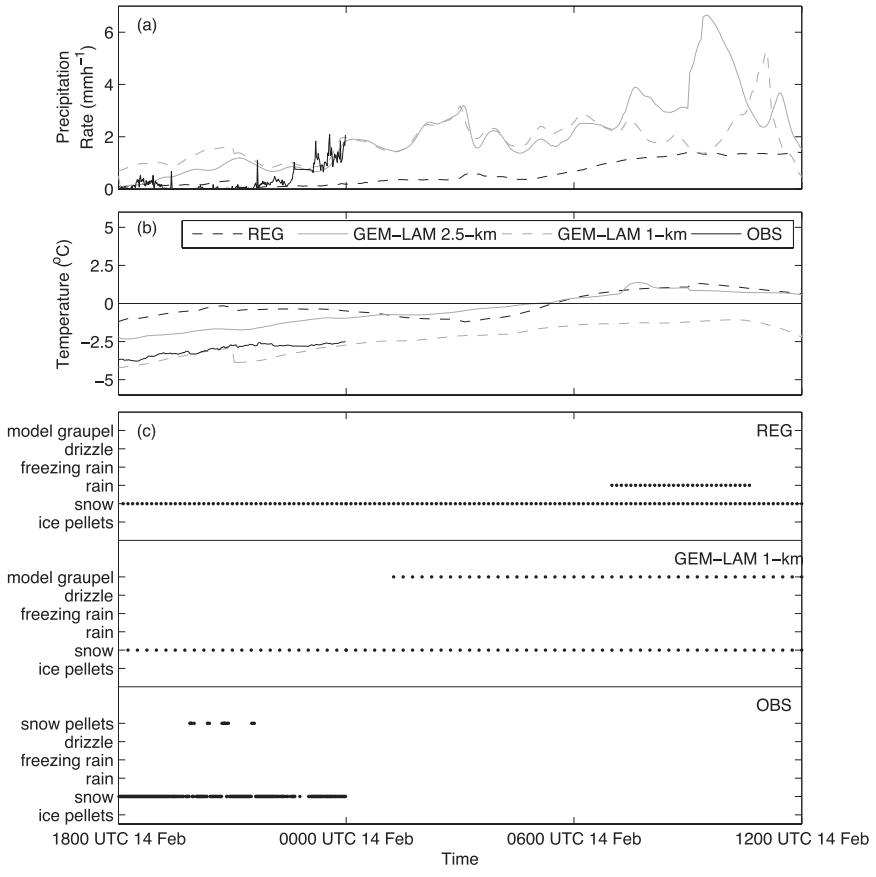

FIG. 4. The (a) precipitation rate and (b) temperature forecasted by the REG, GEM-LAM 2.5-km and GEM-LAM 1-km simulations, and the corresponding observations (OBS) near the top of Whistler Mountain (RND). (c) Precipitation types forecasted by the models and measured by the FD12P optical sensor (OBS). Only the observations up to 0000 UTC 14 Feb 2010 are shown to demonstrate the forecasting challenge.

Whistler Mountain (RND), the GEM-LAM 1-km model suggested temperatures <0°C during the entire period associated with snow, sometimes mixed with graupel (Fig. 4c). The other forecast models suggested that the temperature would rise above 0°C at 0600 UTC. In contrast, all model forecasts suggested temperatures >0°C throughout the storm near the base of Whistler Mountain (VOT). However, the observed temperature near the base of Whistler Mountain at 2000 UTC 13 February 2010 is 2°C higher than the forecasted temperature.

The microphysics parameterization utilized for these high-resolution model predictions was the double-moment version of the scheme developed by Milbrandt and Yau (2005a,b). The precipitating hydrometeors predicted by the scheme are hail (ice pellets), graupel (called model graupel in this study), snow, rain, freezing rain (rain at temperatures below 0°C), and drizzle (rain with mean mass diameter <200 μm). On the other hand, the FD12P (Vaisala Oyj, Helsinki, Finland) measures snow pellets, which could be comparable to model graupel, and an algorithm is used to determine the other types of precipitation (Sheppard and Joe 2000). It also measures, rain, freezing rain, drizzle, snow, and ice pellets. This forecast temperature gradient along the mountainside suggests a transition in precipitation types between the top and base of Whistler Mountain (Figs. 4c and 5c). Because the precipitation phase is very sensitive to the air temperature and because it was always around 0°C, the models were in disagreement over the phase. The conflicting model forecasts illustrate the challenge to forecasting temperature and the precipitation phase distribution in space and time along the mountainside.

The synoptic situation and the operational forecast suggested that a precipitation transition from snow to rain would occur along Whistler Mountain, but its location and timing were unclear. Because the forecasted temperatures were around 0°C and associated with

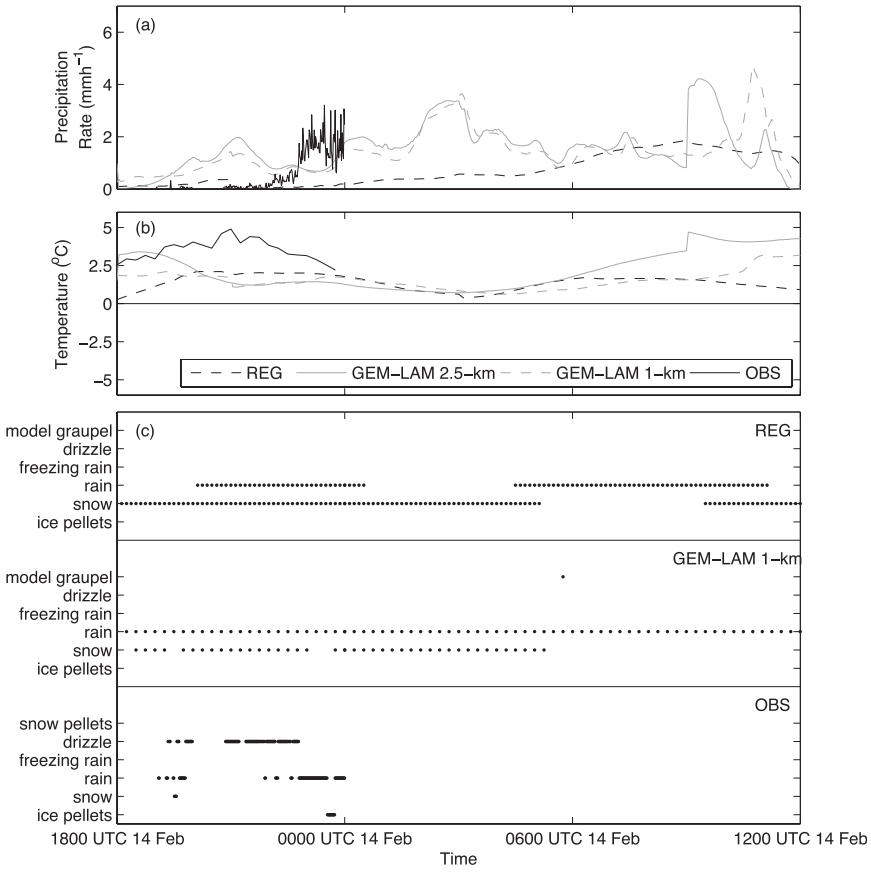

FIG. 5. The (a) precipitation rate and (b) temperature forecasted by the REG, GEM-LAM 2.5-km and GEM-LAM 1-km simulations, and measured (OBS) near the base of Whistler Mountain (VOT). (c) The precipitation types forecasted by the REG and GEM-LAM 1-km simulations and measured by the FD12P optical sensor (OBS). Only the observations up to 0000 UTC 14 Feb 2012 are shown to demonstrate the forecasting challenge.

moderate snow, the diabatic effects of melting seemed to play an important role in keeping the temperature at 0°C. Observations collected in the Whistler area, such as in the Callaghan Valley and along Whistler Mountain, as well as radar measurements and soundings, are used to examine this issue.

4. Weather observations in the Whistler area

A detailed analysis of the precipitation phase and intensity, temperature, and wind speed and directions is conducted for the time period between 1800 UTC 13 February and 1200 UTC 14 February 2010.

a. Precipitation occurrence

The occurrence and intensity of precipitation are the key factors necessary to consider for examining the effect of diabatic cooling on the evolution of a storm. The occurrence of precipitation in the Whistler area was investigated using the measured surface precipitation rate and radar reflectivity. Between 1800 UTC 13 February and 1200 UTC 14 February 2010, water equivalents of 8.8–26.9 mm were recorded in the Whistler area (Table 1).

FD12P weather sensors were installed at RND, VOA, VOL and VOT to measure the precipitation rate along the mountainside (Fig. 1c). Figure 6 shows that precipitation began at around 2200 UTC and continued until at least

TABLE 1. The 6-h water equivalent precipitation amount (mm) at VOC, VOL, VOA, and VOD during the event. The locations of each station are indicated in Fig. 1. QPF is quantitative precipitation forecast.

Time (UTC 14 Feb 2010)	VOC	VOL	VOA	VOD
0000	0.6	1.6	0.7	2.8
0600	3.4	5.5	3.2	10.2
1200	4.8	14.2	10.0	13.9
Total	8.8	21.3	13.9	26.9

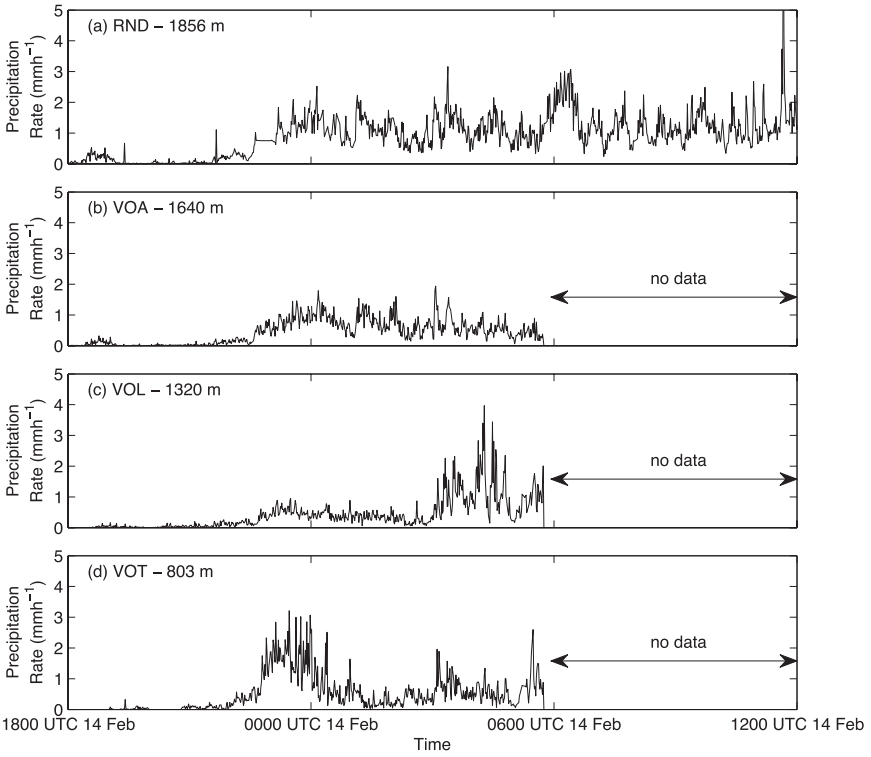

FIG. 6. The 1-min precipitation rate measured by the FD12P along the Whistler Alpine Venue: (a) RND, (b) VOA, (c) VOL, and (d) VOT; the elevation (MSL) of each station is indicated. Note that data at VOA, VOL, and VOT are not available from 0600 to 1200 UTC 14 Feb 2010 due to a power outage.

0600 UTC at a rate of 1–3 mm h^{-1}. The lower precipitation rates observed near the base of Whistler Mountain (VOT) could be due to precipitation evaporation or sublimation. There were no data available from the FD12P sensors for most of the station between 0600 and 1200 UTC 14 February because of a power outage. However, measurements from some other instruments were still available; therefore, the estimations of precipitation amounts during that period are 4.8, 14.2, 10, and 13.9 mm at VOC, VOL, VOA, and VOD, respectively (see Table 1). A larger amount of precipitation was observed at VOD compared to the other stations.

The radar range–height indicator (RHI) cross sections of reflectivity and radial velocity are shown in Fig. 7 (toward the base of Whistler Mountain) and Fig. 8 (toward the Callaghan Valley); the orientations of these two cross sections and the orography of the area are depicted in Fig. 1a. They showed the presence of a bright band aloft, which is usually associated with a melting layer with the maximum reflectivity value (Fabry and Zawadzki 1995). For clarity, we defined a bright band as a narrow band of high reflectivity (35 dBZ or higher), which is generally the level just below the 0°C isotherm. The reflectivity increases when snow starts melting because water droplets form on the lattice structure of the snowflake. Snowflakes are also generally larger in size due to the influence of aggregation at temperatures near 0°C.

The time evolution of the strength and thickness of the radar reflectivity bright band was slightly different in the valleys studied. At 2100 UTC, no precipitation was reported in the region, which was consistent with the low reflectivity value in both the Whistler and Callaghan Valleys. At 0000 UTC, the top-of-radar bright band of 35 dBZ was measured at 1 km (MSL) in both valleys, where the depth of the bright band extended nearly down to the surface. Note that the maximum value reaches 40 dBZ throughout the layer in the Callaghan Valley. At 0300 UTC, the bright band became deeper (up to 1.4 km MSL) and stronger (40 dBZ) near Whistler Mountain. However, the reflectivity maximum value decreased to 30 dBZ in the Callaghan Valley. In both valleys, the height of the bright band increased to almost 1.5 km and thickened considerably. At 1200 UTC the height of the top of the bright band was nearly 1.5 km in both valleys. The stronger radar reflectivity observed in Whistler suggested heavier precipitation at that location as compared to that in the Callaghan Valley.

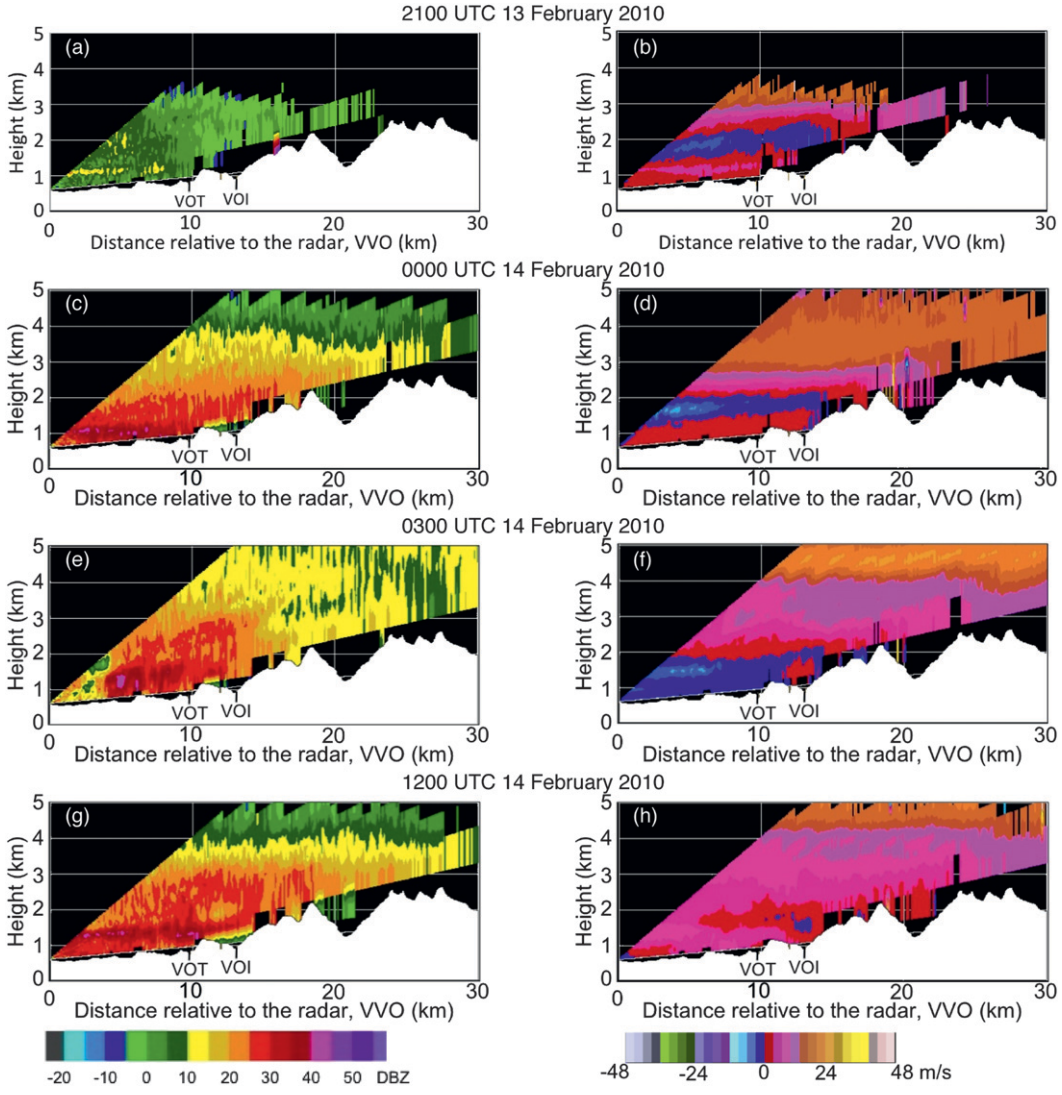

FIG. 7. VVO (left) radar reflectivity and (right) radial velocity cross sections along the 73° line toward VOT near the base of Whistler Mountain for times indicated. The elevation is given as height MSL.

Both radar and surface weather measurements showed precipitation in the Whistler area during the storm. According to the radar reflectivity over Whistler Mountain, a bright band was identified at 1.5 km (MSL), suggesting a melting layer with temperatures around 0°C at this level.

b. Surface temperature time evolution

The time evolution of surface temperature in the Whistler area shows three different patterns (Fig. 9). First, at RND, the temperatures remained below −1°C during the entire event. Second, the temperature was mainly constant at around 0°C at VOA and VOL. However, the temperature at VOL increased slightly at 0600 UTC and decreased at 1200 UTC. Third, at VOI and lower elevations, a maximum temperature was observed at 2100 UTC and then decreased gradually to a constant temperature. For example, at VOI and VOD, the temperature was constant for 4 h at 0°C until it started increasing at 0600 UTC. The increase in temperature was associated with the passage of the warm front. Similarly, at VOT and VOC, the temperature remained steady at 1° and 2.5°C, respectively, instead of 0°C. However, the increase in the temperature is only observed at VOT.

The observed temperature evolution along the mountainside suggests that diabatic cooling of melting snow was dominant during a period of the storm because the temperature was close to 0°C for 3–5 h. The presence of the 0°C isothermal layer can only be

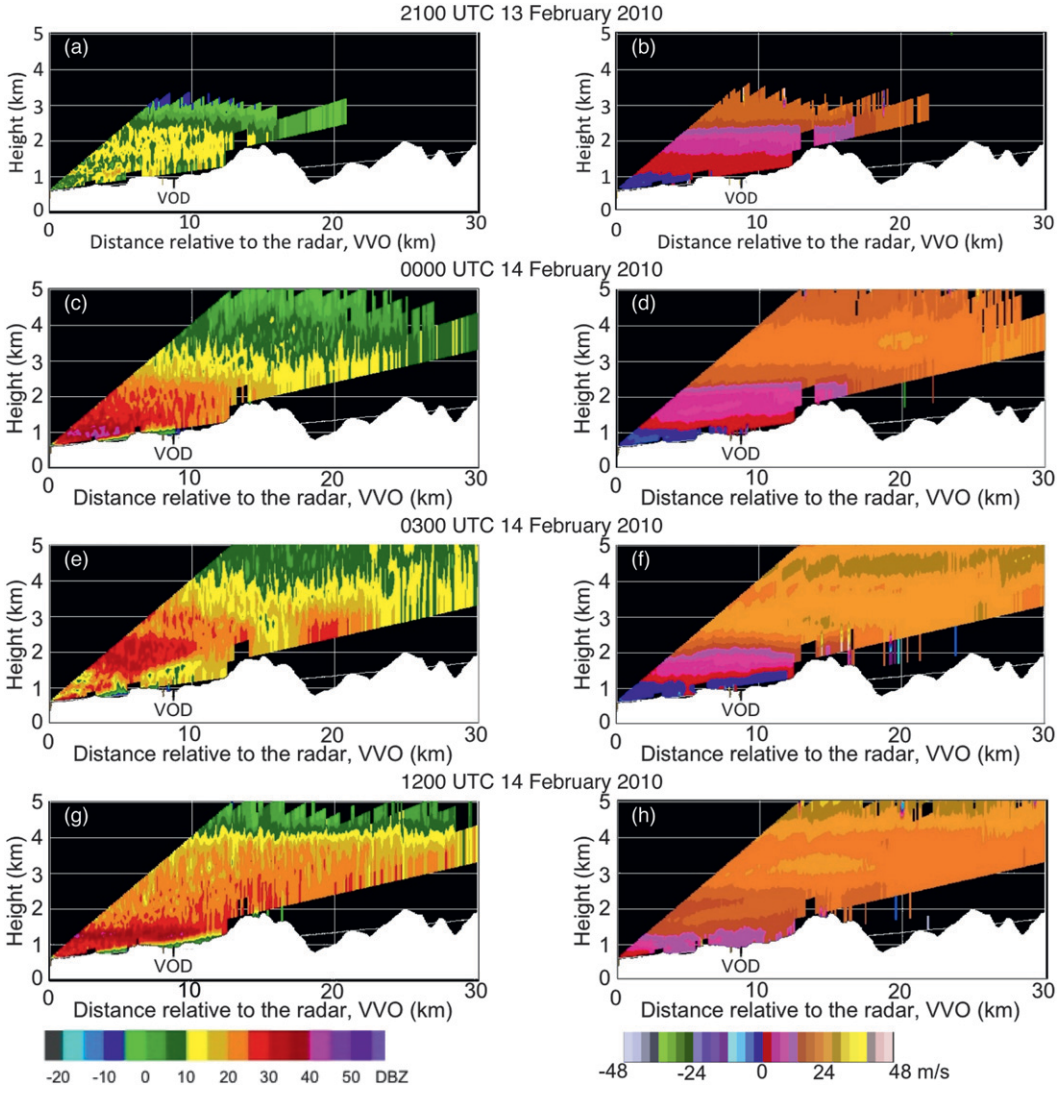

FIG. 8. As in Fig. 7, but for cross sections along the 0° line toward VOD in the Callaghan Valley.

explained through diabatic cooling. The next subsection will analyze the time evolution of vertical temperature and wind profiles to further support these surface observations.

c. *Vertical temperature and wind profiles*

To investigate the role of diabatic cooling and warm-air advection on the ambient temperature, the Whistler soundings launched every 6 h from VOC were analyzed. The vertical temperature and dewpoint temperature profiles are shown in Fig. 10. At 1800 UTC, a shallow melting layer was present near the surface. Later that day (2 h after precipitation started), a melting layer remained near the surface, although the diurnal heating had increased the surface temperature to 4°C. As precipitation fell through the atmosphere, it melted and cooled the air diabatically (at around 0600 UTC). A near-0°C isothermal layer was created between 1000 and 1400 m. At 1200 UTC, the warm-air advection increased the temperature to reach a maximum of 4°C.

From Figs. 10a and 10b, the Whistler sounding showed that the 1800 and 0000 UTC winds were light and variable at lower levels and increased to strong southerly winds aloft. At 0600 UTC, northerly winds started to increase at lower levels with stronger southerly winds aloft (Fig. 10c). At 1200 UTC, the lower-level northerly winds shifted to stronger southerly winds (Fig. 10d), resulting in low-level warm-air advection and a temperature increase.

We should also point out that at 0600 UTC 14 February 2010, an above-freezing layer developed between VOA

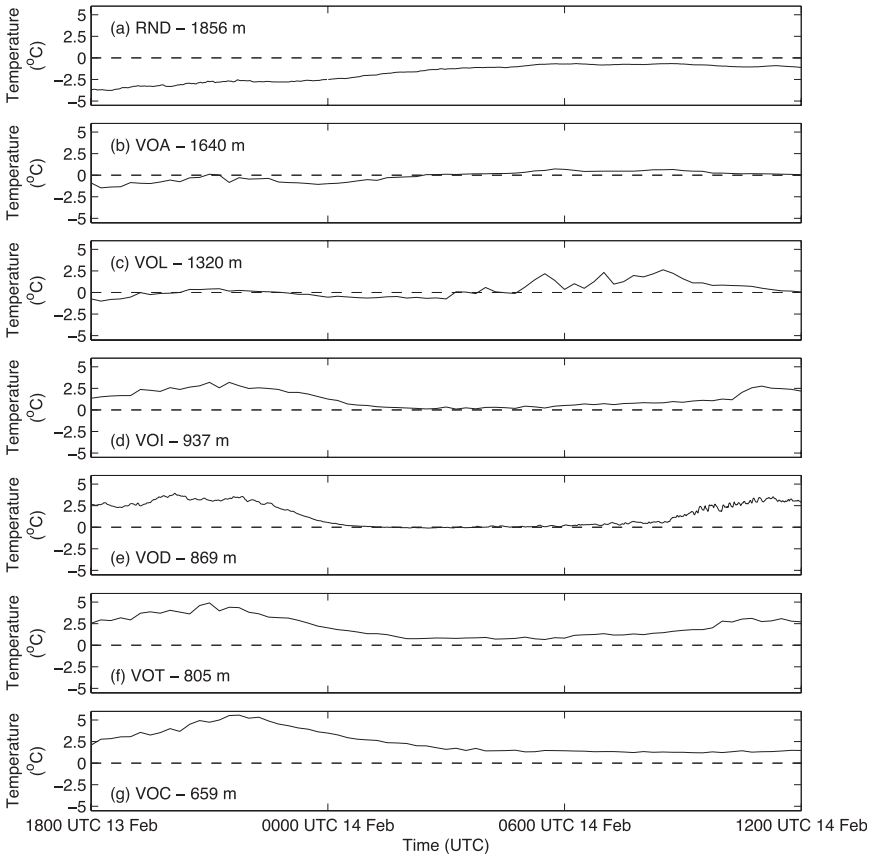

FIG. 9. The 15-min temperature readings at the surface along the Whistler mountainside: (a) RND, (b) VOA, (c) VOL, (d) VOI, (e) VOD, (f) VOT, and (g) VOC; the elevation (MSL) of each station is indicated. The dashed lines indicate the 0°C line at each station.

and VOL (Fig. 10c). The level of the maximum temperature was near a critical level with southerly flow aloft, shifting to northerly flow beneath. That warm layer could have been produced by adiabatic warm through subsidence or by large-scale warm advection. By 1200 UTC, the melting layer was cooled by the diabatic processes of rain evaporation and melting of snow (Fig. 10d).

The time evolution of the soundings suggests that diabatic cooling due to melting snow was dominant between 0000 and 0600 UTC 14 February 2010, except for a shallower layer aloft. The large-scale warm advection became more dominant between 0600 and 1200 UTC when the southerly winds increased at lower levels and contributed to advection of warmer air into the region.

d. Valley flow

The radar radial velocity cross sections scanning over the base of Whistler Mountain (73°) and over the Callaghan Valley (0°) are depicted in Figs. 7 and 8. The direction of the valley flow was different near the base of Whistler Mountain than that in the Callaghan Valley at 0000 UTC. The near-surface down-valley flow occurred in the Callaghan Valley, but not in the Whistler Valley. The down-valley flow near Whistler Mountain was located above the bright band, suggesting that it could be related to the down-valley flows from the two elevated valleys lying to the south and the north of Whistler Mountain, which are perpendicular to the 73° RHI display with valley bottoms higher than 1 km MSL (Fig. 1). At 0300 UTC, both valley flows were also similar (Figs. 7f and 8f) to their 0000 UTC counterparts, but the down-valley flow near Whistler Mountain was 500 m thicker than that in Callaghan Valley. In both valleys, however, the elevation of the shear layer, where the down-valley flow changed to up valley with height, was associated with the top-of-the-radar-reflectivity bright band. The dense cool air produced by the melting snow could have produced a change in the flow direction near the surface. Finally, an up-valley flow was observed in both valleys at 1200 UTC (Figs. 7h and 8h).

The examination of the radar radial velocity in the Whistler Valleys shows that there was a transition from

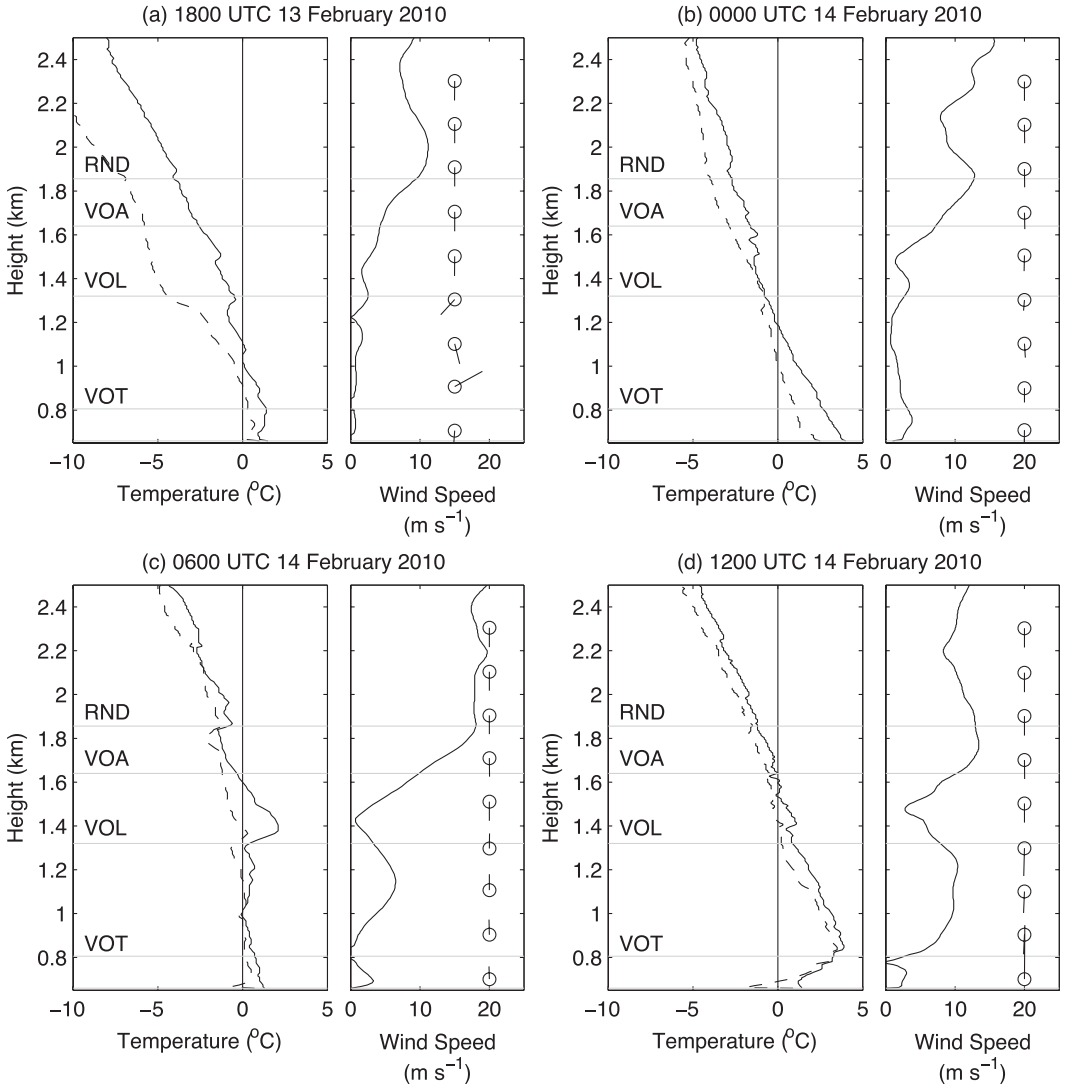

FIG. 10. The vertical temperature (solid line) and dewpoint temperature (dashed line) profiles at (a) 1800 UTC 13 Feb 2010, and at (b) 0000, (c) 0600, and (d) 1200 UTC 14 Feb 2010. The soundings were launched from the Whistler Valley (VOC). The elevations of the weather stations are indicated by the gray lines. Wind bars indicate the direction from which the winds are blowing. The elevation is given as height MSL.

up-valley flow prior to the onset of precipitation to down-valley flow after the onset. This pattern suggests that the diabatic cooling of precipitation affected the atmospheric conditions at the beginning of the event (until 0600 UTC). The flow switched to up valley when the warm southerly winds started to dominant the diabatic cooling effects at 1200 UTC and created a change in the flow direction near the surface. However, in the Callaghan Valley, the flow was oriented down valley at 2100 UTC, but by looking at the accumulated precipitation (Table 1), that region had already received 3 times the amount compared to the stations located in the Whistler Valley.

e. Surface precipitation–type evolution

The temperatures and valley flow in the Whistler area described in the above sections suggest the occurrence of a precipitation-type transition associated with height and time. It is difficult to measure solid or a mixture of solid and liquid precipitation because they fall at different terminal fall velocities and have different shapes (Thériault et al. 2012). The precipitation type and rate were evaluated by the FD12P sensors installed at the RND,VOA, VOL, and VOT sites (Fig. 1b). Note that optical precipitation sensors can easily detect snow or rain, but are not as accurate for mixed precipitation.

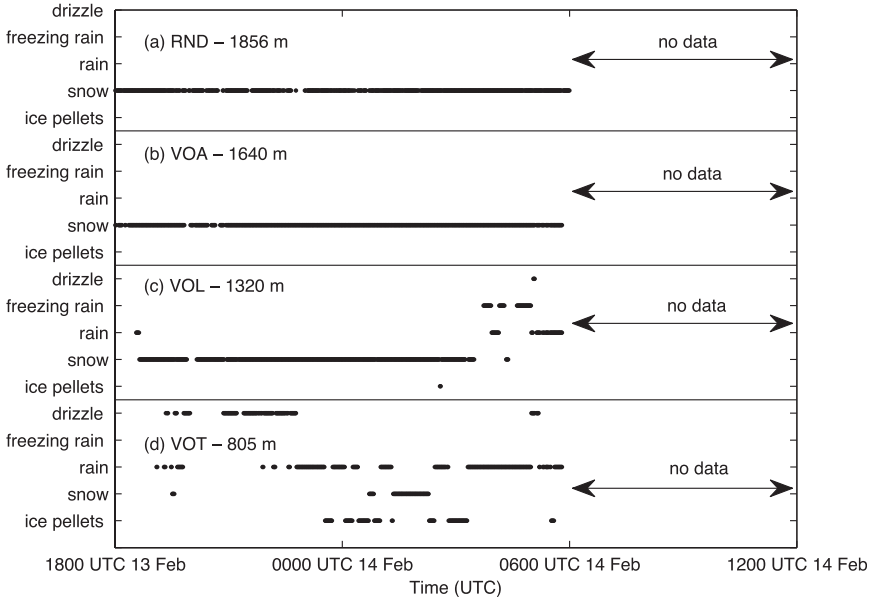

FIG. 11. The time evolution of surface precipitation types at different elevations along Whistler Mountain between 1800 UTC 13 Feb 2010 and 1200 UTC 14 February 2010: (a) RND, (b) VOA, (c) VOL, and (d) VOT; the elevation (MSL) of each station is indicated. Data were not available after 0600 UTC because of a power outage.

A precipitation-type transition region was measured along the mountainside (Fig. 11). Snow was observed to fall at high-elevation stations (RND and VOA), consistent with the temperature being ≤0°C at these locations (cf. Fig. 9). Near the base of the mountain (VOT), the precipitation type was mostly liquid, as reported by the instruments, due to the above-freezing temperature during the entire event. However, when the temperature was near 0°C at around 0200 UTC, a mixture of precipitation types (snow, freezing rain, and ice pellets) was reported by the instruments at VOT. At midelevation (VOL), snow was measured until 0400 UTC 14 February 2010. At that time, the temperature increased slightly to 2°C and the precipitation type changed to rain. This precipitation transition moved up the mountainside consistent with temperature changes along the mountain transect and the sounding (Figs. 9 and 10c).

5. Comparison of the observations with the model forecasts

As discussed in Mailhot et al. (2010), during the Vancouver 2010 Winter Olympics forecasters had access to a special Olympic mesoscale prediction system consisting of a cascade of three one-way nested grids of GEM-LAM. The GEM-LAM 1-km model run will be compared to the observations at both Whistler Mountain and the Callaghan Valley. Further description of the forecast configuration is given in appendix B.

a. Surface weather condition

As shown in Figs. 12a and 13a, the model predicted the start of precipitation earlier than reported by the observations. However, when it started, the predicted precipitation rates were similar to the observed rates at RND but slightly lower than the observed rates at VOT. Due to the power outage at 0600 UTC 14 February 2010, no precipitation was recorded at VOL and VOT. The precipitation instrument (FD12P) situated at RND was not affected. After 0600 UTC, the precipitation rates measured at RND were less than the predicted rates with a nearly constant value of 2 mm h^{-1}. At 1100 UTC the GEM-LAM 1-km simulation predicted the maximum precipitation rate (5.2 mm h^{-1}), which was more than 3 times higher than the observed rate. The rate of 6.8 mm h^{-1} recorded shortly after than may be an artifact in the data.

The surface temperatures predicted by the GEM-LAM 1-km model near the top and base of the mountainside are shown in Figs. 12b and 13b. At RND, the model forecast temperatures <0°C throughout the period, which was consistent with the observations. Near the base of the mountain (VOT), the model did not predict the temperature increase observed at 2100 UTC. This could be due to the overforecast of cloud cover. For example, the model predicted precipitation at that time, which implies cloudy conditions, whereas precipitation was only observed during a later period. When precipitation

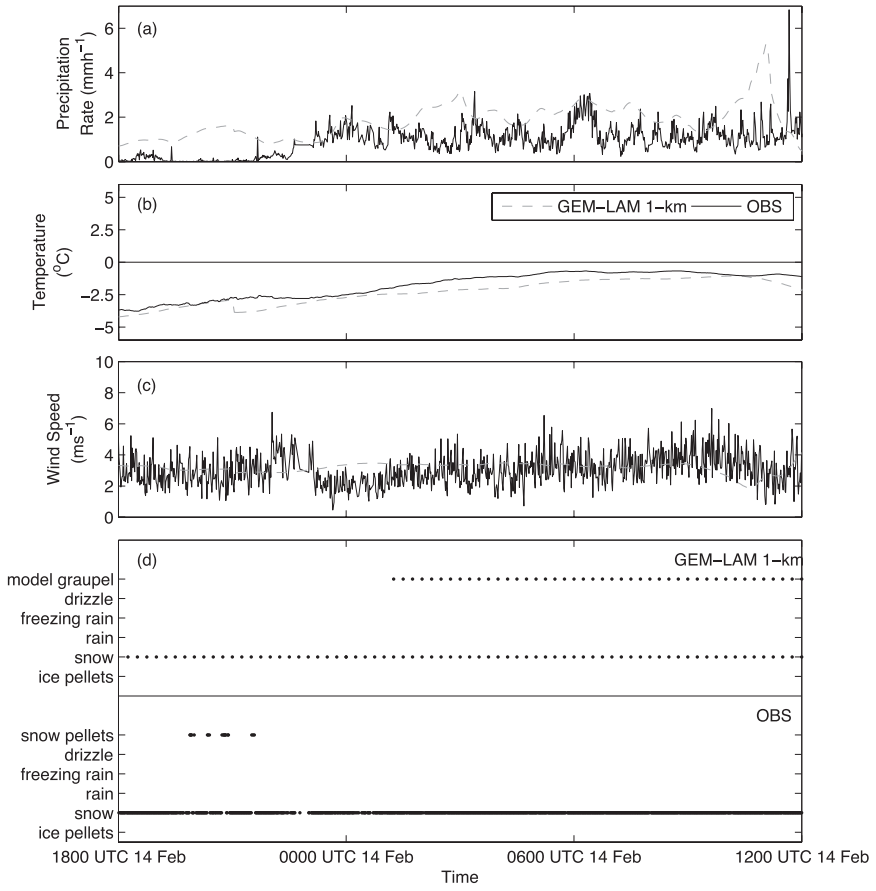

FIG. 12. A comparison of the model forecasts (GEM-LAM 1-km) and observations of the (a) precipitation rate, (b) temperature, and (c) wind speed and (d) precipitation types near the top of Whistler Mountain (RND). The precipitation rate was measured by an FD12P optical sensor. The legend is the same for all panels.

started, the agreement between the model forecasts and the observations improved. The temperature decreased to near 1°C and increased again after 0600 UTC. In Callaghan Valley (Fig. 14a), the temperatures followed the same trends as observed and predicted at VOT. However, the predicted temperature never reached 0°C, as reported by the instruments at VOD.

Wind speed was not well predicted by the model at lower elevations compared to higher elevations in the Whistler area during the storm. First, the wind speed value predicted by the GEM-LAM-1 km model near the top of Whistler Mountain (Fig. 12c) was similar to the observations. Second, the model-forecasted 1 m s^{-1} wind speed at VOD differed only slightly from the observations (~0 m s^{-1}). However, the predicted wind speeds increased to 3–4 m s^{-1} after 0900 UTC, which agreed well with the observations. The increase in the wind speed was well correlated with a sharp increase in temperature. Note that calm conditions were observed in the Callaghan Valley between 2300 and 0600 UTC. This may partially explain the poor prediction of temperature by the model at VOD. Stronger wind speeds will lead to a smaller impact of diabatic cooling due to melting snow because temperature advection dominates (Unterstrasser and Zängl 2006; Minder et al. 2011). However, lower wind speed will diminish the impact of advection on the temperature and lead to a different temperature trend. Third, the predicted wind speed pattern at VOT is different than in the Callaghan Valley. They were constant throughout the storm at 1–2 m s^{-1}, whereas the observations showed variable winds <1 m s^{-1}.

Because the temperature evolution along the mountainside oscillated around 0°C, the determination of the precise precipitation type was difficult. Figures 12d and 13d compare precipitation types observed against the model (GEM-LAM 1-km) forecast near the top (RND) and the base (VOT) of Whistler Mountain [see Milbrandt and Yau (2005a,b) for the description of model precipitation categories]. At RND (Fig. 12d), the model

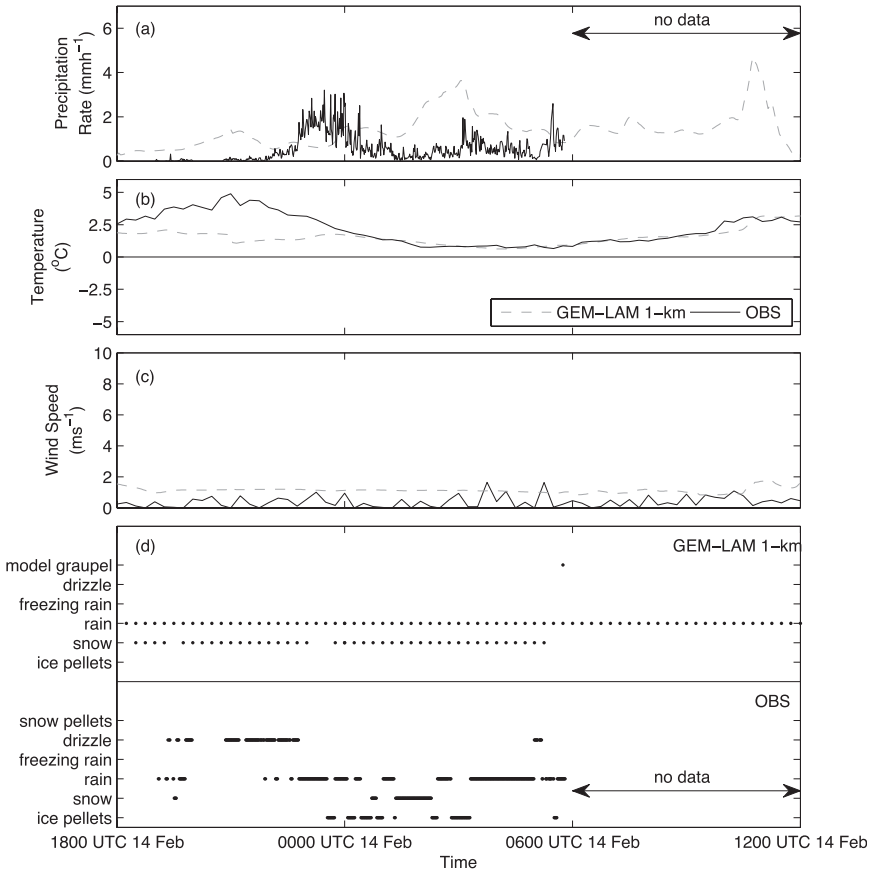

FIG. 13. A comparison of the model forecasts (GEM-LAM 1-km) and observations of the (a) precipitation rate, (b) temperature, (c) wind speed, and (d) precipitation types near the base of Whistler Mountain (VOT). The precipitation rate was measured by an FD12P optical sensor. The legend is the same for all panels. Note that wind speed is represented by 15-min data due to the power outage.

predicted a mixture of graupel and snow at the surface with below 0°C temperatures, in agreement with the observations of frozen precipitation at that location. Near the base of Whistler Mountain, the temperature remains above 0°C during the entire storm (Fig. 13b). At 2100 UTC, the model predicted a rain–snow mix whereas the instruments reported rain or drizzle (Fig. 13d). This was likely due to the actual temperature being 2°C warmer than the model forecast, which led to the complete melting of snow and produced rain in the valley. Between 0000 and 0600 UTC, a mixture of rain and snow was predicted by the GEM-LAM 1-km model, as was also reported by the instruments.

In general, the GEM-LAM 1-km forecast was able to reproduce the observations, especially at higher elevations.

b. Valley flow comparison

The valley flows simulated by the model and measured by the radar are compared in this section. The GEM-LAM 1-km model simulations of the radar reflectivity and radial velocity along the cross sections through the base of Whistler Mountain and the Callaghan Valley are shown in Figs. 15 and 16, respectively.

The total equivalent radar reflectivity is the sum of the equivalent reflectivity from each of the five noncloud

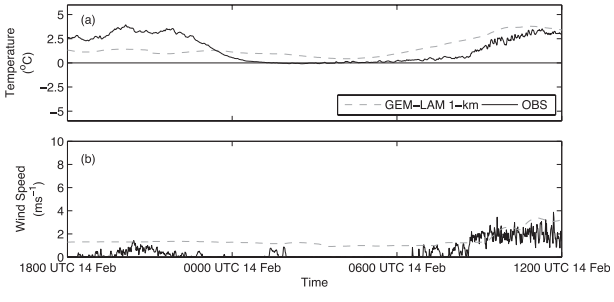

FIG. 14. A comparison of the model forecasts (GEM-LAM 1-km) and observations of the (a) temperature and (b) wind speed in the Callaghan Valley (VOD). The legend is the same for all panels.

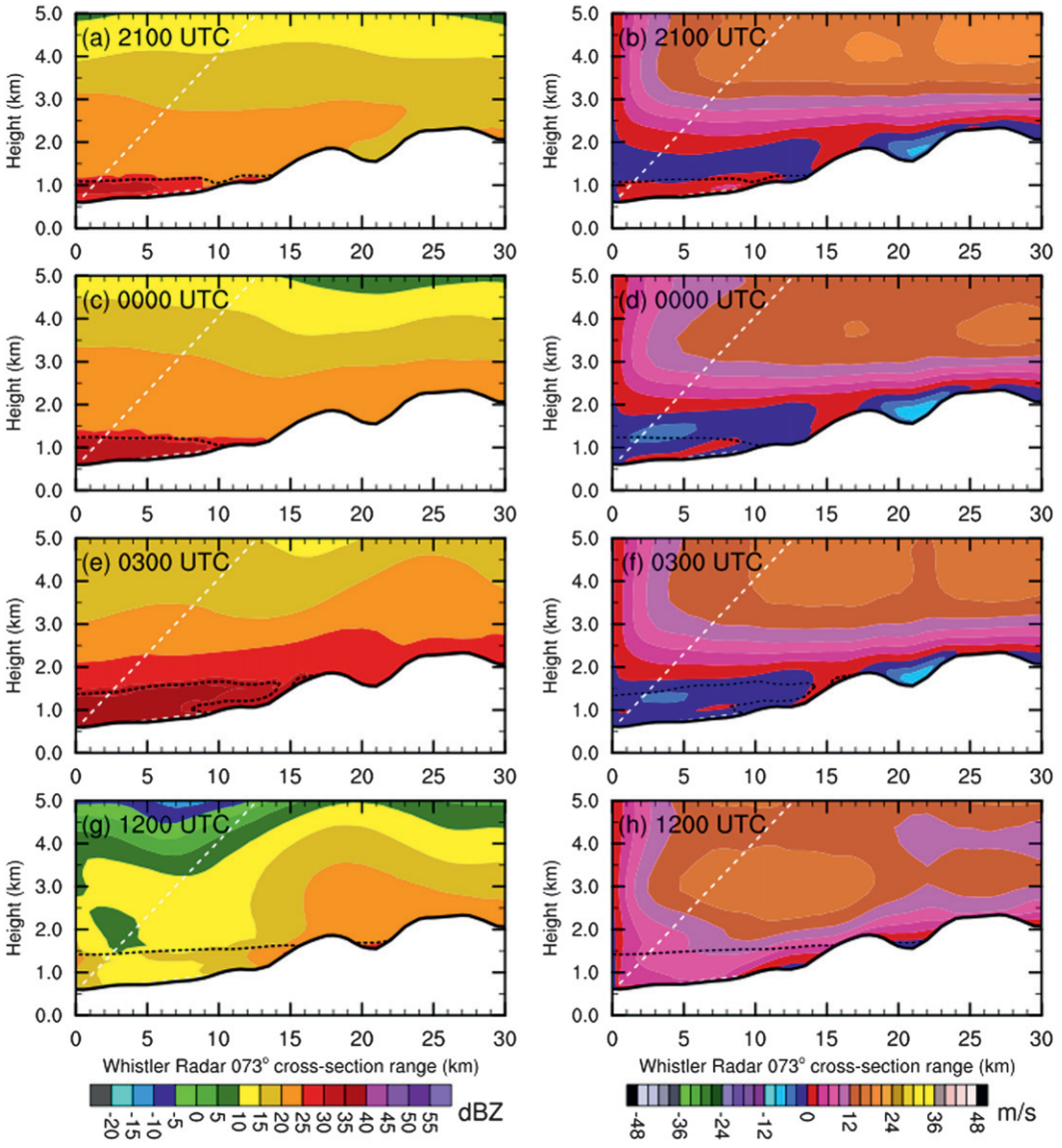

FIG. 15. VVO radar cross sections of the (left) total equivalent reflectivity and (right) radial velocity, predicted by the GEM-LAM 1-km model initialized at 2000 UTC 13 Feb 2010. The cross sections are along the 73° line toward VOT near the base of Whistler Mountain. The black dashed line indicates the freezing level (0°C isotherm). The white dashed lines mark the sector that can be compared with the radar observations in Fig. 7. The elevation is given as height MSL.

hydrometeor categories computed by the double-moment version of the Milbrandt–Yau bulk microphysics scheme (Milbrandt and Yau 2005a,b; Milbrandt et al. 2008). The computation makes a simple estimate for the brightband effect, which may not be accurate enough to duplicate the observed radar bright band. The equivalent Doppler radar radial velocity is calculated by projecting the three-dimensional hydrometeor velocity on the slanted direction of the radar beam, based on the assumption that the atmospheric refractivity index varies linearly with height (Doviak and Zrnić 1993).

To highlight the freezing level, the height of the 0°C isotherm is added to Figs. 15 and 16. It is shown that the freezing level increased from 1.2 to 1.5 km during the storm. At 0000 UTC, the height of the freezing level (top of the melting layer) was higher than the height of the maximum observed reflectivity but was at a comparable height at 0300 and 1200 UTC (Figs. 7 and 8). The soundings (cf. Fig. 10) show that the height of the melting layer increased from 0000 to 0600 UTC. This height increase was comparable to the real radar reflectivity (Figs. 7 and 8) but the model simulations stayed nearly constant

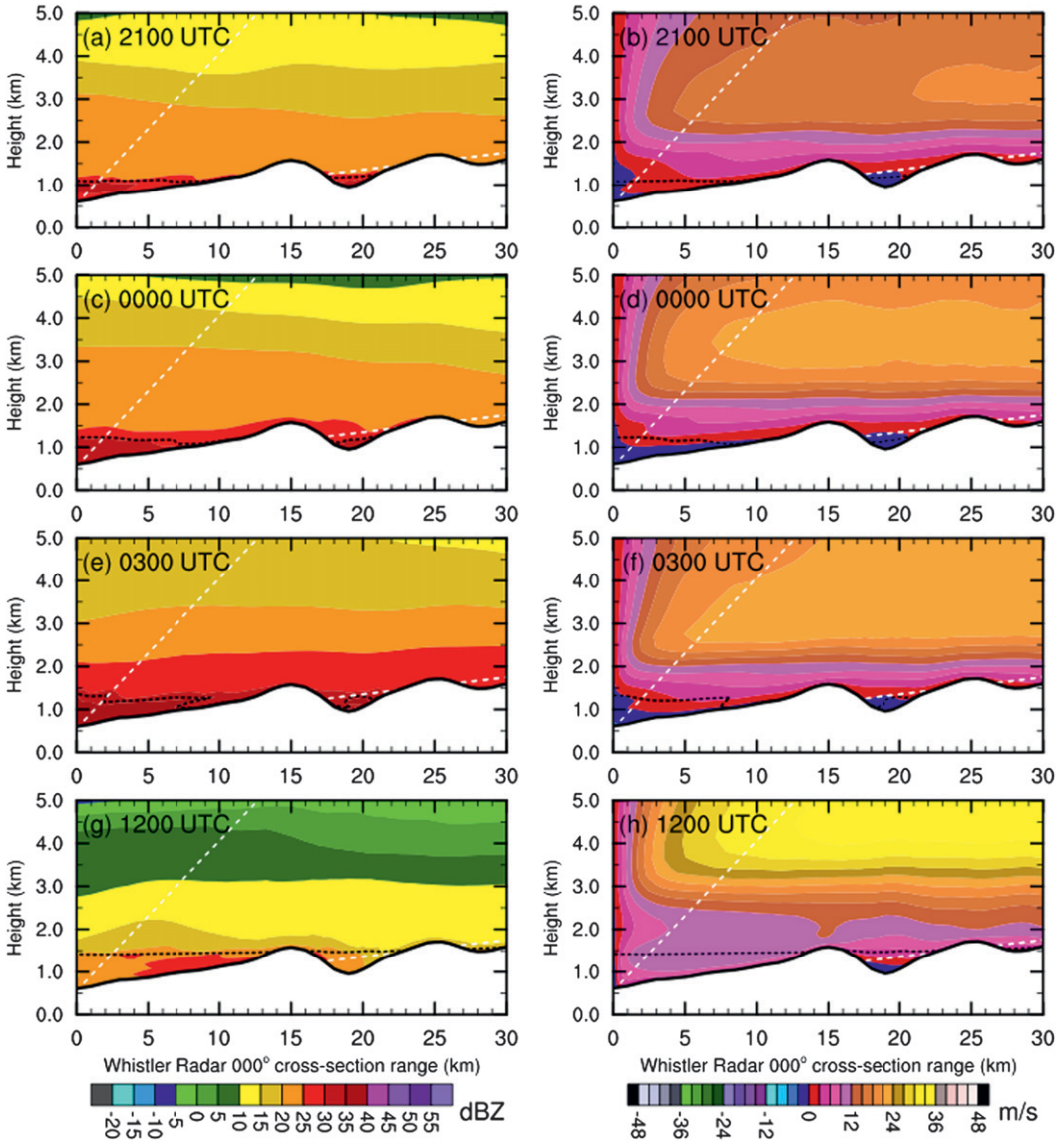

FIG. 16. As in Fig. 15, but for cross sections along the 0° line toward VOD in the Callaghan Valley.

with time. The vertical temperature profiles are simulated and are discussed further in section 6.

There are a few inconsistencies in the model radial velocity cross section. At 0000 UTC, the model airflow was comparable to the observations, but the radar-measured depth of the down-valley flow was thicker than the model-predicted depth. At 0300 UTC, the direction of the predicted flow was comparable to the radar measurements. In the Callaghan Valley, the measured down-valley flow extended up to 15 km north of the radar whereas the model only reproduced the down-valley flow up to 5 km. At 1200 UTC, the predicted valley flow was similar to the radar measurement. Both model and radar data showed up-valley flow associated with the passage of the front over the area.

The near-surface valley flows predicted by the GEM-LAM 1-km model are plotted in Fig. 17. These are the winds at 10 m above the surface at those grid points with elevations below 1000 m MSL. It is shown that down-valley flow in the Whistler area began to develop soon after the onset of precipitation at 2200 UTC 13 February 2010 (Fig. 17a), and persisted at least until 0600 UTC 14 February (Figs. 17b–e). The up-valley flow spread into the Callaghan Valley around 0800 UTC (Fig. 17f). But it took until 1200 UTC (Fig. 17h) to reach the base of Whistler Mountain (VOT) and the up-valley flow was only observed at VOC at 1400 UTC (Fig. 17i).

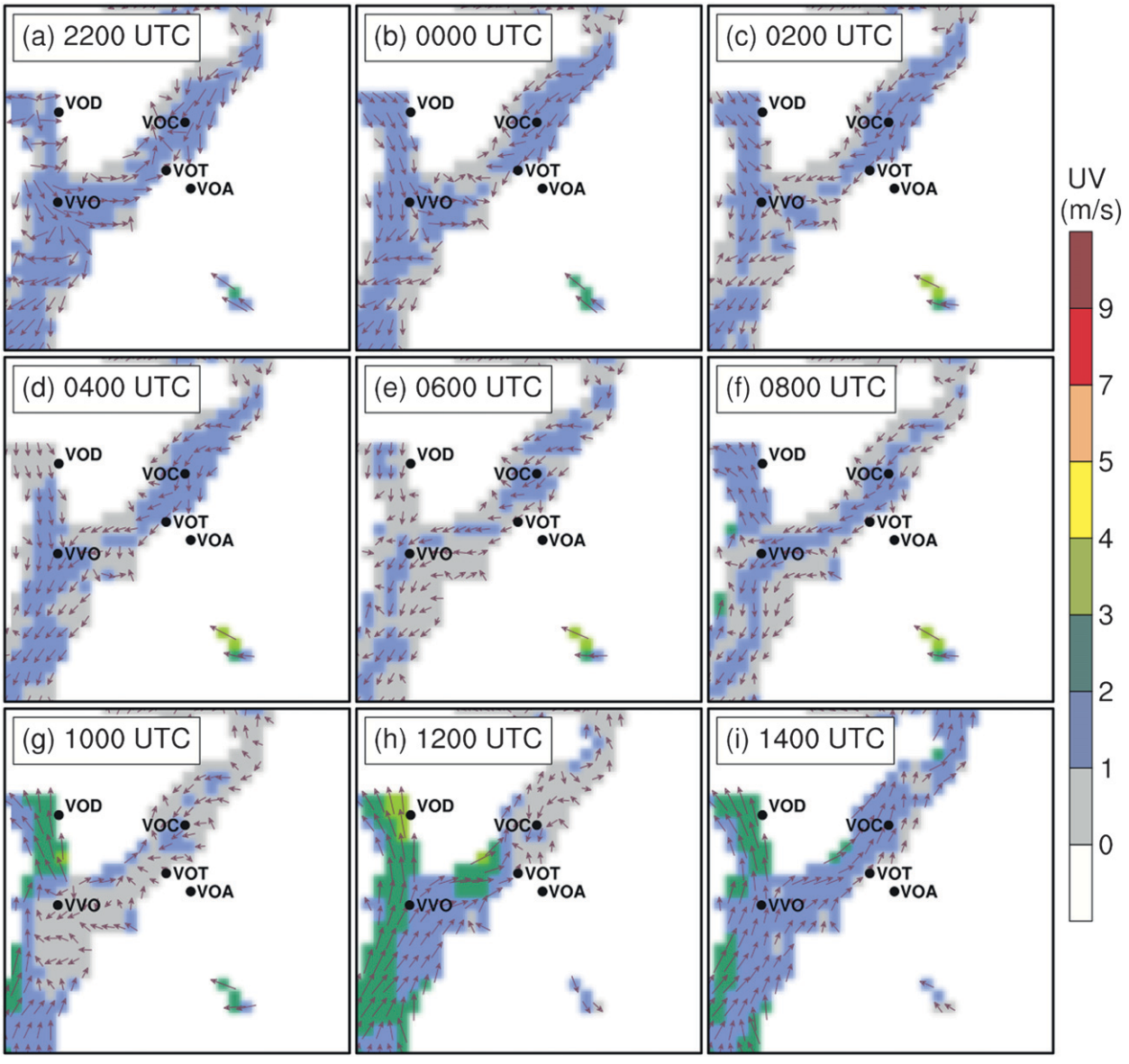

FIG. 17. Winds at 10 m above the surface, predicted by the GEM-LAM 1-km model initialized at 2000 UTC 13 Feb 2010. Only 10-m winds at those grid points with elevations below 1000 m MSL are plotted.

6. Sensitivity experiments

So far, the comparison of observations with the high-resolution NWP model results has been used to illustrate the significance of diabatic cooling of melting snow. It has been shown that the time period impacted by the melting snow (0000–0600 UTC) was associated with calm winds at lower altitudes and stronger winds aloft. As the effect of diabatic cooling of melting snow decreased, the winds started to increase and shifted direction in association with the passage of a warm front. In this section, one-dimensional (1D) numerical simulations were performed to support the evidence of diabatic cooling during this period of the storm.

a. 1D kinematic cloud model

A kinematic 1D cloud model coupled with a sophisticated bulk microphysics scheme was developed by Thériault and Stewart (2010). This bulk microphysics scheme is based on the double-moment scheme of Milbrandt and Yau (2005a,b) that has a sophisticated parameterization of winter precipitation types (e.g., melting and freezing processes). Wind effects (i.e., horizontal wind speed, vertical air velocity, and

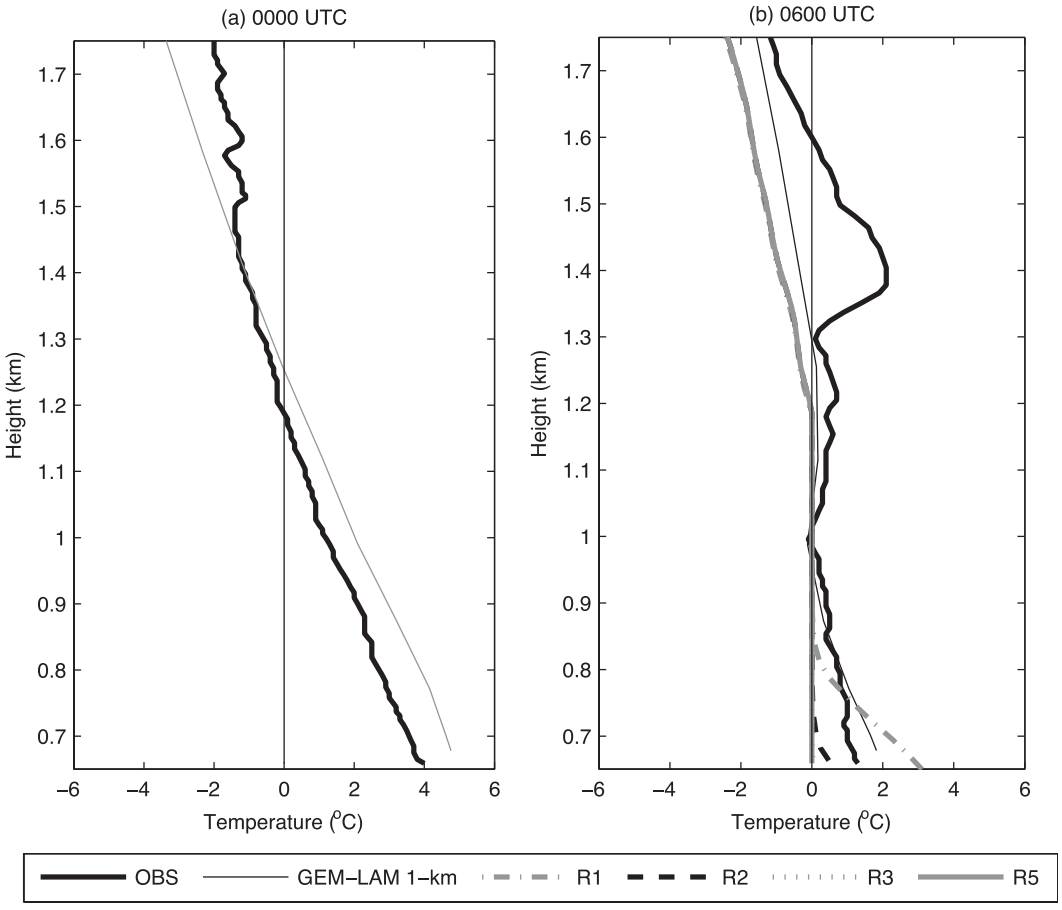

FIG. 18. Comparison of the GEM-LAM 1-km (solid black line) and the measured (boldface solid black line) temperature profiles above VOC at (a) 0000 and (b) 0600 UTC. The simulated temperature profiles obtained from the 1D simulations are shown in (b) and with assumed precipitation rates of 1, 2, 3, and 5 mm h^{-1} for R1, R2, R3, and R5, respectively. Elevation is given as height MSL. Note that the vertical temperature profiles associated with precipitation rates $\geq$3 mm h^{-1} led to an isothermal layer of 0°C (i.e., curves R3 and R5 are superimposed).

convective over turning) were neglected in this simulation due to the nearly calm conditions between 0000 and 0600 UTC.

The 1D model was initialized with the 0000 UTC 14 February 2010 sounding (temperature and humidity profiles; Fig. 10b) launched from VOC. It was assumed that snow falls continuously from above the melting layer at 2.5 km MSL to the freezing level at 1.2 km MSL. The time and space evolution of the vertical temperature profile, cooling rates of the environment, and surface precipitation–type evolution were simulated by varying the initial precipitation rate (1, 2, 3, and 5 mm h^{-1}). These values were chosen to represent the actual rates observed during the storm, which varied between 1 and 3 mm h^{-1} .The higher rate of 5 mm h^{-1} was chosen for comparison. The model was run for 6 h so that comparison can be made between the simulated and observed vertical temperature profiles at 0600 UTC. The time evolution of precipitation types and temperature variations between 0000 and 0600 UTC for different locations will also be compared with corresponding surface observations.

b. Vertical temperature profile

The vertical temperature profile measured by the sounding launched at VOC is compared to the GEM-LAM 1-km forecast sounding in Fig. 18a. Both of the vertical temperature profiles showed a 550-m-deep above-freezing layer ($T > 0$°C, also called a melting layer) near the surface, with a surface temperature around 5°C. The dewpoint is not shown but the atmosphere was mostly subsaturated aloft in both cases. Figure 18b shows the corresponding predicted (GEM-LAM 1-km model) and observed (sounding) vertical temperature profiles at 0600 UTC. The sounding shows a melting layer with a maximum temperature of 2°C between 1.3 and 1.5 km, which was not predicted by the GEM-LAM 1-km model.

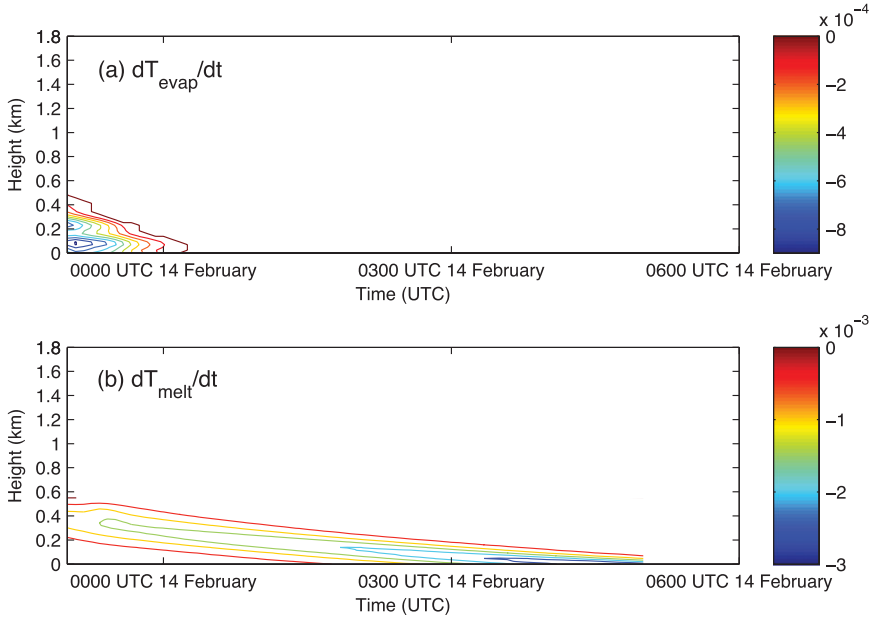

FIG. 19. Cooling rate (°C s^{-1}) due to diabatic cooling from (a) evaporation and (b) melting assuming a 2 mm h^{-1} initial snowfall rate. The elevations are heights above ground with respect to VOC (659 m MSL).

The results from the 1D sensitivity study are compared with the 0600 UTC sounding and the GEM-LAM 1-km forecast at the same time. Figure 18b shows the temperature profile obtained after 6 h assuming four different precipitation rates. The differences between the different precipitation rate cases are noticeable at heights <0.9 km. A deep 0°C isothermal (0.4 km) layer was produced by a precipitation rate of 1 mm h^{-1}. The depth of the isothermal layer increased with increasing precipitation rate. For example, a 2 mm h^{-1} precipitation rate produced a 0.5-km 0°C isothermal layer and precipitation rates >3 mm h^{-1} produced an 0°C isothermal down to the surface. Finally, the warmer layer between 1.3 and 1.5 km MSL was not simulated by both the GEM-LAM 1-km and one-dimensional models. It is probably due to the fact that the winds were not correctly predicted in the GEM-LAM 1-km simulation and that the 1D simulations did not consider warm-air advection and other processes.

The results of the 1D simulations with different precipitation rates provide a plausible explanation for the different temperatures observed at VOD (0°C) and VOT (1°C). At a precipitation rate of 2 mm h^{-1}, the 1D simulations suggest a surface temperature of ~0.5°C at VOT whereas VOD is slightly cooler at 0°C. However, if the precipitation rates were lower at VOT than at VOD, the surface temperature at VOT would be higher because it would be less affected by the diabatic cooling of melting snow. As shown in Table 1, the precipitation amount in the Whistler Valley was less than in the Callaghan Valley during this time period.

The observed precipitation rates were, on average, between 2 and 3 mm h^{-1} during the storm (Fig. 6). The 1D simulated temperature profiles produced by precipitation rates of 2 and 3 mm h^{-1} are similar at altitudes below 1.3 km (Fig. 18). As the precipitation rate increases, the depth of the 0°C isothermal layer increases. In all of the cases studied, the atmosphere was saturated at 0600 UTC, which was comparable to the observed weather conditions. Therefore, the 1D simulations suggest that the diabatic cooling of melting snow exerted a major influence on the evolution of the storm between 0000 and 0600 UTC at lower elevations. However, because the lower elevations were subsaturated at 0000 UTC, the diabatic cooling of rain evaporation was more intense than the effect of melting snow during the first 60 min (Fig. 19a). After that time, the diabatic cooling of melting snow intensified and lasted through the entire time period, resulting in further cooling (Fig. 19b).

According to the VOC sounding, other processes led to an increase in temperature at higher altitudes between 1.3 and 1.5 km, which cannot be explained with the 1D model study. The observed warming could be caused by the leeside subsidence as the southerly winds descended along the northern slope of Whistler Mountain and adiabatically heated the air in the valley (e.g., Mo et al. 2012).

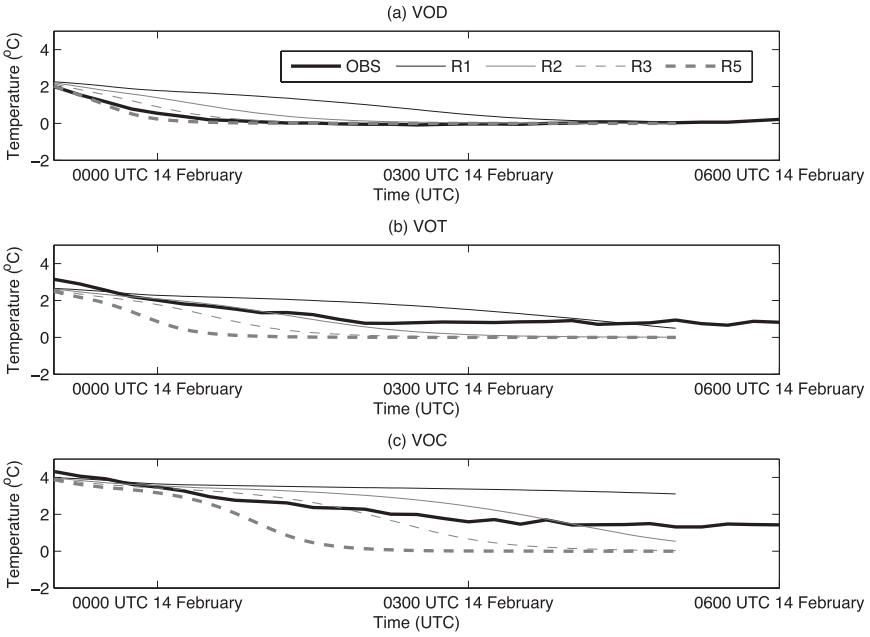

FIG. 20. A comparison of the simulated and observed temperature variations for three locations in the Whistler area: (a) VOD at 869 m MSL in the Callaghan Valley, (b) VOT at 805 m MSL near the base of Whistler Mountain, and (c) VOC at 659 m MSL in the Whistler Valley.

c. Temperature variation

The simulated and observed temperature variations at three different Olympic venues are compared in Fig. 20. Since that temperature quickly dropped between 0000 and 0600 UTC 14 February 2010, the measured temperature by the sounding and at the stations (VOC, VOT, and VOD) was more comparable at 2300 UTC rather than at 0000 UTC. This is consistent with the fact that soundings are generally launched from the surface 45 min before the hour. Therefore, the analyzed temperature time series in Fig. 20 started at 2300 UTC 13 February 2010 and were compared with the one-dimensional cloud model simulations during a 6-h period.

The simulated temperatures only agreed with the observations for the first 2–3 h of the simulation at VOT and VOC. If the temperature had not reached 0°C, the simulated temperature would keep decreasing whereas the observations suggested a constant temperature. This could be due to a bias in the temperature measurements, to the temporal variation of the precipitation rate during that time period (Fig. 6), or to the presence of other atmospheric processes that kept the temperature above 0°C. For example, subsidence (adiabatic warming) might have been generated by the cool dense air produced by the diabatic cooling of melting snow or by the southerly large-scale flow. This process could have influenced the temperature and humidity at lower elevations. Finally, the temperature variations produced by precipitation rates of 3 and 5 mm h^{-1} were more comparable to the observations. It should also be noted that more precipitation were reported at VOD (Table 1), where the diabatic cooling of melting snow appears to be more evident than at VOC (Table 1) and VOT (Fig. 6).

For all three stations, the temperature decrease for the 1 mm h^{-1} rate is slower than those from higher precipitation rates. As the initial precipitation rate increases, the temperature decreases at a faster rate because more heat is absorbed during the melting process. Furthermore, the cooling rate increases with height. As snow falls from aloft, it starts to melt when reaching the top of the melting layer. When falling through the melting layer, the mass of snow is gradually converted into rain. Because the mass of snow decreases as it falls through the melting layer, the diabatic cooling effect on the environmental temperature also decreases. This is the reason why the cooling rate at lower elevations is less than at higher elevations in this case. The observations demonstrated similar results. It is possible that convective overturning may be triggered by an unstable layer produced by diabatic cooling of snow at the top of the melting layer and redistribute the cooling over a shallow layer. Further investigations should be conducted into this issue.

7. Concluding remarks

Forecasting the occurrence and intensity of precipitation associated with a winter storm on 13–14 February 2010 was a great challenge due to the near-freezing temperature profile in the Whistler area. This study analyzes in detail the observations and model predictions of this high-impact storm, with focus on the diabatic cooling effect due to snow melting over the complex mountainous terrain.

The Olympic Autostation Network (Joe et al. 2010, JPAG) and the SNOW-V10 project (IPAG) provided various weather observations at a very high spatial–temporal resolution. The detailed observations at some stations in the Whistler area, together with special radar data and high-resolution NWP outputs (GEM Regional-15 km, GEM-LAM 2.5-km, and GEM-LAM 1-km), provided a unique dataset that was used in this study to diagnose the thermodynamic and microphysics processes related to the storm evolution. Our analysis of the observations provided strong evidence of diabatic cooling leading to snow instead of rain near the base of Whistler Mountain during the early part of the storm, with warm advection becoming more influential during the later period.

The GEM-LAM 1-km model was able to capture most of the observed features in terms of temperature as well as precipitation rates and types. However, there were differences in the timing of the precipitation, precipitation rates, wind speed, and temperature that may have affected the storm evolution. The GEM-LAM 1-km model showed considerable promise as a tool for improving forecasting of diabatic processes in complex terrain. In particular, it captured the diabatic cooling of melting snow and the formation of down-valley flow when the diabatic cooling occurred.

The 1D sensitivity study conducted with the bulk microphysics scheme coupled with a kinematic cloud model suggested the dominating role of diabatic cooling between 0000 and 0600 UTC 14 February 2010. The simulations showed that the precipitation rate affected the evolution of the temperature profile and led to a vertical conversion of the melting layer into a 0°C isothermal layer. It was also noted that evaporation contributed to cooling the environmental air at the onset of precipitation as the atmosphere was subsaturated at lower levels near the surface. This temperature evolution directly affected the precipitation type by stopping the melting process and allowing only solid precipitation to reach the ground. Other parameters, such as large-scale forcing, could be added to the 1D simulations to compute the effects of warm-air advection at different elevations to investigate specific conditions where diabatic cooling may be important when competing with large-scale warm advection.

It is conceivable that warm, moist southerly flow may have been channeled through the Sea-to-Sky corridor and then partially blocked by the local topography in the Whistler area (see Fig. 1). Under stable conditions a weak reversed downslope flow can be produced (e.g., Smolarkiewicz et al. 1988; Rasmussen et al. 1989; Mo et al. 2012), which may initiate a secondary surface cold front to enhance the orographic precipitation aloft. Because of the presence of the melting layer near the surface, the precipitation aloft would undergo phase changes and alter the environmental temperature. In addition, the southerly flow over Whistler Mountain may lead to subsidence on its north side, which could contribute to the warming of the environmental air. Besides this possible local adiabatic warming, the data analysis suggests that diabatic temperature changes from precipitation processes significantly affect the environmental conditions. Hence, if a secondary cold front was induced by flow blocking, it would have been significantly reinforced by the diabatic cooling due to rain evaporation, and then by melting snow that lasted for about 6 h (in particular in the Callaghan Valley). These diabatic cooling effects result in the formation of cold air on the mountain. This cold dense air likely contributed to the switch from up-valley to down-valley flow. During later periods of the event, the valley flow likely switched back to up-valley flow as the warm-air advection became dominant over diabatic processes. Further sensitivity studies are necessary in order to quantify the relative contribution of diabatic processes with respect to flow blocking, adiabatic effects, and large-scale temperature advection on the direction of the valley flow.

Overall, this study demonstrated the important impacts diabatic cooling due to evaporating and melting snow can have on the phase of the winter precipitation during a storm. Accurate parameterization of such diabatic processes needs to be included in models to improve winter precipitation forecasts. This is particularly important for winter storms in regions where the ambient temperature is close to 0°C. The issue of forecasting precipitation phase and intensity was critical for safe and fair competitions during the Vancouver 2010 Olympic Winter Games.

Acknowledgments. We thank the Advanced Study Program (ASP), the Research Applications Laboratory (RAL), the Water System Program at the National Center for Atmospheric Research (NCAR), as well as Environment Canada for the financial support needed to accomplish this work. The National Center for Atmospheric Research is sponsored by the National Science Foundation.

APPENDIX A

Instrumentation during SNOW-V10

Besides the conventional observations, the research sites were equipped with specialized instruments. A comprehensive description of the observing network is provided by JPAG. Relevant observed weather elements and instrumentation for this study include the following:

- disdrometers (Parsivel by OTT; POSS by All Weather Instruments) for particle size, distribution, particle fall velocity, and precipitation type by inference;
- vertically pointing radar (Micro Rain Radar by METEK), which produced vertical profiles of reflectivity, vertical particle velocity, and Doppler spectra;
- visibility (FD12P and PW22D by Vailsala, Belfort 6210) and inferred from Parsivel data; and
- high-resolution precipitation intensity and type (POSS by All Weather Instruments, FD12P and PWD22 by Vaisala, Hot Plate by Yankee, Pluvio2 by OTT); the latter two instruments did not produce precipitation type.

APPENDIX B

Model Configuration during SNOW-V10

The dynamical core for Environment Canada's Olympic mesoscale deterministic prediction system is based on the Global Environmental Multiscale (GEM) model (Côté et al. 1998), version 4.0.6, run in the limited-area model (LAM) configuration (Mailhot et al. 2010, MPAG). This version uses a hybrid terrain-following, log-pressure-based vertical coordinate and a vertical discretization based on Charney–Phillips staggering; 58 vertical levels were used. There are 13 levels in the lowest 2 km where the melting process usually occurs. Model runs consisted of a one-way nested cascade of GEM-LAM grids, with 15-, 2.5-, and 1-km horizontal grid spacings, referred to as LAM-15, LAM-2.5, and LAM-1, respectively. Two sets of simulations were run daily, initialized from the 0000 and 1200 UTC Canadian Meteorological Centre (CMC) regional analyses, with lateral boundary conditions supplied from CMCs operational regional (15 km) forecast runs, every 6 h. In this study, only the second run is examined. The nesting times are illustrated in Fig. B1.

The GEM-LAM simulations used the following physics parameterizations: the double-moment version of the Milbrandt and Yau (2005a,b) bulk microphysics scheme to treat grid-scale clouds and precipitation, the Kain–Fritsch scheme to parameterize deep convection (LAM-15 only; no convective parameterization scheme was used in the LAM-2.5 or LAM-1), the Òmoist-TKEÓ scheme to treat boundary later turbulence (Bélair et al. 1995), the Lin and Barker (2005) correlated-*k* radiative transfer scheme, and the Interactions between Soil, Biosphere, and Atmosphere (ISBA) land surface scheme (Bélair et al. 2003). For further details on the model configuration, please see MPAG.

The model time series were constructed with output every time step (30 s for the LAM-1) and grid points chosen to be the most representative for each station. In most cases, this was the nearest grid point, but for some locations it was deemed to be more appropriate to use another nearby model grid point that more closely matched the station in terms of elevation and wind exposure. Precipitation rates were computed at the lowest prognostic model level; near-surface temperatures and dewpoint temperatures (2 m) and winds (10 m) were diagnosed by the model (to the given diagnostic level, relative to the orographic height as seen by the model).

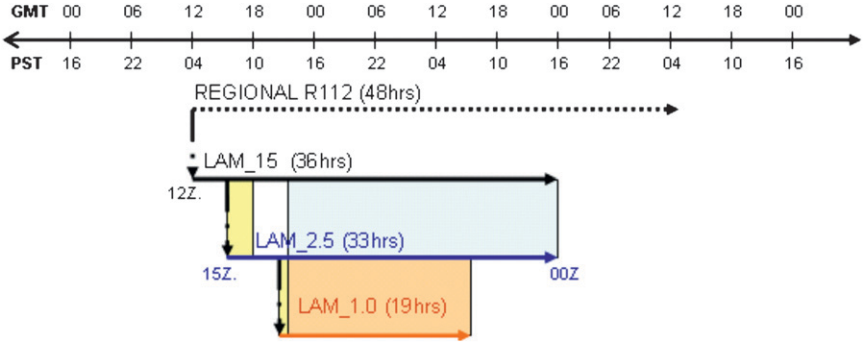

FIG. B1. Model integration and nesting times for the second daily run of the high-resolution GEM-LAM modeling system for the Vancouver 2010 Winter Olympics. [Modified from MPAG.]

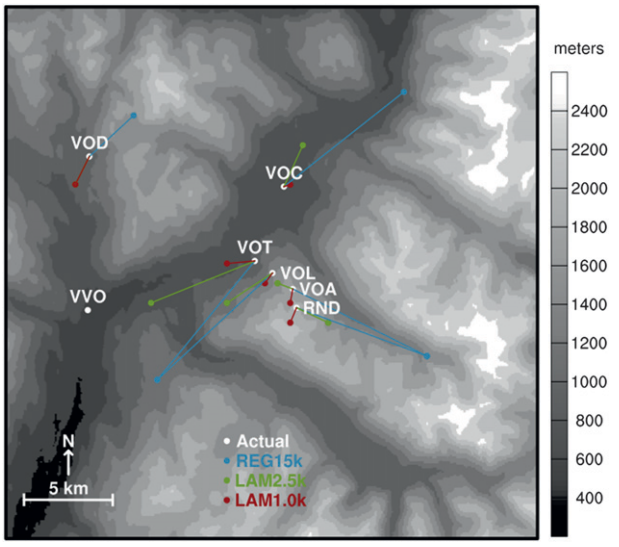

FIG. B2. The comparisons of model grid points (REG 15-km, GEM-LAM 2.5-km, and GEM-LAM 1-km) and the actual geographical locations of the Olympic weather stations in the Whistler area.

The locations of the grid points for the three model configurations and the geographical locations of the weather stations in the Whistler area are shown in Fig. B2.

REFERENCES

Bélair, S., J. Mailhot, C. Girard, and P. Vaillancourt, 1995: Boundary layer and shallow cumulus clouds in a medium-range forecast of a large-scale weather system. *Mon. Wea. Rev.,* **133,** 1938–1960.

——, L. P. Crevier, J. Mailhot, B. Bilodeau, and Y. Delage, 2003: Operational implementation of the ISBA land surface scheme in the Canadian regional weather forecast model. Part I: Warm season results. *J. Hydrometeor.,* **4,** 352–370.

Côté, J., S. Gravel, A. Méthot, A. Patoine, M. Roch, and A. Staniforth, 1998: The operational CMC–MRB Global Environmental Multiscale (GEM) model. Part I: Design considerations and formulation. *Mon. Wea. Rev.,* **126,** 1373–1395.

Doviak, R., and D. Zrnić, 1993: *Doppler Radar and Weather Observations.* 2nd ed. Academic Press, 562 pp.

Fabry, F., and I. Zawadzki, 1995: Long-term radar observations of the melting layer of precipitation and their interpretation. *J. Atmos. Sci.,* **52,** 838–851.

Findeisen, C., 1940: The formation of the 0°C isothermal layer and fractocumulus under nimbostratus. *Meteor. Z.,* **54,** 49–54.

Gultepe, I., G. A. Isaac, P. Joe, P. A. Kucera, J. M. Thériault, and T. Fisico, 2012: Roundhouse (RND) mountain top research site: Measurements and uncertainties for Alpine weather conditions. *Pure Appl. Geophys.,* in press.

Isaac, G. A., and Coauthors, 2012: Science of Nowcasting Olympic Weather for Vancouver 2010 (SNOW-V10): A World Weather Research Programme project. *Pure Appl. Geophys.,* doi:10.1007/s00024-012-0579-0, in press.

Joe, P., and Coauthors, 2010: Weather services, science advances, and the Vancouver 2010 Olympic and Paralympic Winter Games. *Bull. Amer. Meteor. Soc.,* **91,** 31–36.

——, and Coauthors, 2012: The monitoring network of the Vancouver 2010 Olympics. *Pure Appl. Geophys.,* in press.

Lin, J., and H. W. Barker, 2005: Radiation algorithm with correlated-*k* distribution. Part I: Local thermal equilibrium. *J. Atmos. Sci.,* **62,** 286–309.

Lumb, F. E., 1983a: Sharp snow/rain contrast—An explanation. *Weather,* **38,** 71–73.

——, 1983b: Snow on hills. *Weather,* **38,** 114–115.

Lundquist, J. D., P. J. Neiman, B. Martner, A. B. White, D. J. Gottas, and F. M. Ralph, 2008: Rain versus snow in the Sierra Nevada, California: Comparing Doppler profiling radar and surface observations of melting level. *J. Hydrometeor.,* **9,** 194–211.

Mailhot, J., and Coauthors, 2010: Environment Canada's experimental numerical weather prediction systems for the Vancouver 2010 Winter Olympic and Paralympic Games. *Bull. Amer. Meteor. Soc.,* **91,** 1073–1085.

——, J. A. Milbrandt, A. Giguère, R. McTaggart-Cowan, A. Erfani, A. Glazar, and M. Vallée, 2012: An experimental high-resolution forecast system during the Vancouver 2010 Winter Olympic and Paralympic Games. *Pure Appl. Geophys.,* doi:10.1007/s00024-012-0520-6, in press.

Marwitz, J. D., 1987: Deep orographic storms over the Sierra Nevada. Part I: Thermodynamic and kinematic structure. *J. Atmos. Sci.,* **44,** 159–173.

Medina, S., B. F. Smull, R. A. Houze, Jr., and M. Steiner, 2005: Cross-barrier flow during orographic precipitation events: Results from MAP and IMPROVE. *J. Atmos. Sci.,* **62,** 3580–3598.

Milbrandt, J. A., and M. K. Yau, 2005a: A multimoment bulk microphysics parameterization. Part I: Analysis of the role of the spectral shape parameter. *J. Atmos. Sci.,* **62,** 3051–3064.

——, and ——, 2005b: A multimoment bulk microphysics parameterization. Part II: A proposed three-moment closure and scheme description. *J. Atmos. Sci.,* **62,** 3065–3081.

——, ——, J. Mailhot, and S. Belair, 2008: Simulation of an orographic precipitation event during IMPROVE-2: Part I: Evaluation of the control run using a triple-moment bulk microphysics scheme. *Mon. Wea. Rev.,* **136,** 3873–3893.

Minder, J. R., D. R. Durran, and G. H. Roe, 2011: Mesoscale controls on the mountainside snow line. *J. Atmos. Sci.,* **68,** 2107–2127.

Mo, R., and Coauthors, 2012: Mid-mountain clouds at Whistler during the Vancouver 2010 Winter Olympics and Paralympics. *Pure Appl. Geophys.,* doi:10.1007/s00024-012-0540-2, in press.

Ralph, F. M., P. J. Neiman, G. A. Wick, and C. S. Velden, 2004: Satellite and CALJET aircraft observations of atmospheric rivers over the eastern North Pacific Ocean during the winter of 1997/98. *Mon. Wea. Rev.,* **132,** 1721–1745.

Rasmussen, R. M., P. K. Smolarkiewicz, and J. Warner, 1989: On the dynamics of Hawaiian cloud bands: Comparison of model results with observations and island climatology. *J. Atmos. Sci.,* **44,** 1589–1608.

Sheppard, B., and P. Joe, 2000: Automated precipitation detection and typing in winter: A two-year study. *J. Atmos. Oceanic Technol.,* **17,** 1493–1507.

Smolarkiewicz, P. K., R. M. Rasmussen, and T. L. Clark, 1988: On the dynamics of Hawaiian cloud bands: Island forcing. *J. Atmos. Sci.,* **45,** 18721905.

Steiner, M., R. A. H. O. Bousquet, B. F. Smull, and M. Mancini, 2003: Airflow within major Alpine river valleys under heavy rainfall. *Quart. J. Roy. Meteor. Soc.,* **129,** 411–431.

Stoelinga, M. T., and Coauthors, 2003: Improvement of Microphysical Parameterization through Observational Verification Experiment (IMPROVE). *Bull. Amer. Meteor. Soc.,* **84,** 1807–1826.

Thériault, J. M., and R. E. Stewart, 2010: A parameterization of the microphysical processes forming many types of winter precipitation. *J. Atmos. Sci.,* **67,** 1492–1508.

——, R. M. Rasmussen, K. Ikeda, and S. Landolt, 2012: Dependence of snow gauge collection efficiency on snowflake characteristics. *J. Appl. Meteor. Climatol.,* **51,** 745–762.

Unterstrasser, S., and G. Zängl, 2006: Cooling by melting precipitation in Alpine valleys: An idealized numerical modelling study. *Quart. J. Roy. Meteor. Soc.,* **132,** 1489–1508.

Wexler, R., R. J. Reed, and J. Honig, 1954: Atmospheric cooling by melting snow. *Bull. Amer. Meteor. Soc.,* **35,** 48–51.

Zängl, G., 2007: Reversed flow in the south-Alpine Toce Valley during MAP-IOP 8: Further analysis of latent cooling effects. *Quart. J. Roy. Meteor. Soc.,* **133,** 1717–1729.

Zhu, Y., and R. E. Newell, 1998: A proposed algorithm for moisture fluxes from atmospheric rivers. *Mon. Wea. Rev.,* **126,** 725–735.